Spring 2022

Structural, Electrical and Optical Properties of Copper Oxide Phase Mixture: An Active Layer of Solar Cell

Rifat Ara Shams
Missouri State University, Shams26@live.missouristate.edu

STRUCTURAL, ELECTRICAL AND OPTICAL PROPERTIES OF COPPER OXIDE PHASE MIXTURE: AN ACTIVE LAYER OF SOLAR CELL

A Master's Thesis

Presented to

The Graduate College of

Missouri State University

In Partial Fulfillment

Of the Requirements for the Degree

Master of Science, Materials Science

By

Rifat Ara Shams

May 2022

STRUCTURAL, ELECTRICAL AND OPTICAL PROPERTIES OF COPPER OXIDE PHASE MIXTURE: AN ACTIVE LAYER OF SOLAR CELL

Materials Science

Missouri State University, May 2022

Master of Science

Rifat Ara Shams

ABSTRACT

Both CuO and Cu_2O have been well studied and implemented individually as an active layer of a solar cell from early age of manufacturing. A mixture of these two-phase contents at different ratios can bring variance in absorbance which can present new and diverse aspect in solar cell fabrication with added efficiency. Previous works were successful to vary the phase mixture, and the nanostructures provided very high absorption co-efficient but poor optical response on electrical conductivity. The goal of this research is to find out the optimum parameter for the phase mixture of copper oxide with high absorption coefficient as well as good optical response on electrical conductivity. Pulsed laser deposition and subsequent controlled annealing have been used to find the optimum phase mixture of copper oxide thin films to maximize the opto-electrical conductivity and absorption in the solar spectrum. To obtain the structure-property correlation, X-ray diffraction, Raman spectroscopy, scanning electron microscopy, opto-electronic transport measurements, and UV-VIS spectroscopy were carried out on thin film samples. Owing to the change in the phase content in the copper oxide thin films some consistent variations in the electrical and optical properties have been observed. And so far, a thin film copper oxide phase mixture (CuO 87.30%, Cu_2O 12.70%) with a thickness of 200 nm yielded an absorption co-efficient of 3.0E+5 cm^{-1} which is greater than that of a standard CuO (1.19E+5 cm^{-1}), and also a large change in electrical conductivity with light has been found. This phase mixture with the maximum absorption coefficient and large opto-electronic response can be implemented as an active layer of a solar cell which would help attaining maximum efficiency in copper oxide-based heterojunction solar cell. To understand the opto- electronic properties, band structure calculation on copper oxide was also performed using density functional theory.

KEYWORDS: solar cell, phase mixture, absorption, electrical, optical, copper oxide, pulsed laser deposition

STRUCTURAL, ELECTRICAL AND OPTICAL PROPERTIES OF COPPER OXIDE PHASE MIXTURE: AN ACTIVE LAYER OF SOLAR CELL

By

Rifat Ara Shams

A Master's Thesis
Submitted to the Graduate College
Of Missouri State University
In Partial Fulfillment of the Requirements
For the Degree of Master of Science, Materials Science

May 2022

Approved:

Kartik Ghosh, Ph.D., Thesis Committee Chair

Ridwan Sakidja, Ph.D., Committee Member

Tiglet Besara, Ph.D., Committee Member

Julie Masterson, Ph.D., Dean of the Graduate College

ACKNOWLEDGEMENTS

At first, I would like to thank my supervisor **Dr. Kartik Ghosh** and one of the faculty of PAMS department, **Dr. Ridwan Sakidja** for their guidance without which this thesis would have been impossible to accomplish. I specially want to thank **Jacob Berry** for his assistance with a mention worthy part of this project. I am grateful to **Dr. Anagh Bhaumik** and **Dr. Ariful Haque** for their time and valuable opinion on various aspect of the research. Last but not the least, I would like to thank my colleagues **Md. Zia Uddin Mahmud** and **Md. Shaihan Bin Iqbal Emon** for their help regarding this thesis whenever I needed. My heartiest thanks to all of you for helping me to reach this proud moment of accomplishment.

I dedicate this thesis to my late father **Md. Shamsul Haque**, who always encouraged me to chase my dream and my mother **Fatema Begum** who never forgets to put my name in her prayers

TABLE OF CONTENTS

LIST OF TABLES

LIST OF FIGURES

INTRODUCTION

Renewable Energy

The source for renewable energy is natural resources, and they are replenishable over a period on their own without draining the Earth's resources. These resources are rich in nature and available everywhere, and they cause little, if any, damage to the environment or human civilization. To meet the demand of the rapidly increasing population of the earth, all available technologies are shifting their dependency from fossil fuel to renewable energy. There are many shortcomings of using fossil fuels like limited supply, threatening the environment with the emission of greenhouse gases like CO_2. That is why modern technologies are being dependent on alternates like the use of fossil fuels in conjunction with carbon sequestration, nuclear power, and solar power increasingly. But it is a matter of fact that carbon sequestration is quite inconvenient due to its high maintenance and the requirement for large space to store the greenhouse gases that are emitted due to the use of fossil fuel. As sources for renewable energy are limited in supply, non-refillable leaving carbon trace, the whole tech industry is now interested in conducting increased research on solar energy.

The solar to electric conversion process is industrially adapted because of its' viability and less residue. This is a gigantic energy source which has massive solar to electricity conversion power. The total energy supplied by sun in one hour is equivalent to energy needed by humans for a whole year. in one hour. Sun relentlessly supplies 1.2E+25 TW of energy which exceeds the power throughput of other sources. That is the reason that the focus is on particularly solar energy from all renewable energy. But this is not all sunshine for the solar cell industry yet. The main obstacles in the way of solar cells being commercially viable are the high production

costs and the reduction of efficiency. To address this recurring problem with limited efficiency, researchers are putting continuous effort into developing experimental materials with better absorbance at long wavelengths but so far with little success. People has worked on nanoparticle network and tried increasing the nanoparticle film thickness. The motive was improving the absorption in the visible light spectrum. But the electron diffusion length in nanoparticle network also increased parallel to the increment in optical density. That is why it is important to conduct research on the development of unique materials instead of nanoparticles which will have a balance between higher optical absorption coefficient and good conductivity.

Properties of CuO and Cu_2O

Properties of Cu_2O. Copper oxide has three stable phases, and they are Cu_2O, CuO and Cu_2O_3. Among them, Cu_2O crystallizes in a simple cubic Bravais lattice which is shown in figure 1.1. and the crystallographic properties are listed in table 1.1. [2]. Oxygen atoms are four-fold coordinated with copper atoms as nearest neighbors, and copper atoms are linearly coordinated with two oxygen atoms as nearest neighbors. The space group for Cu_2O is Pn3m.

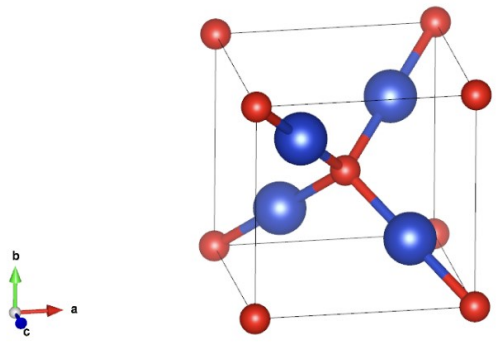

Figure 1.1. Crystal structure of the unit cell of Cu_2O [2]

Table 1.1. Crystallographic properties of Cu2O [3]

Parameter	Standard value
lattice constant	4.2696 ± 0.0010 A˚
space group	Pn3m (224)
bond length Cu–O	1.849 A˚
Separation O–O	3.68 A˚
separation Cu–Cu	3.012 A˚
cell volume	(77.833 ± 0.055) * 10E-24 cm^3
Formula weight	143.14
density	5.749–6.140 g/cm^3
melting point	1235°C

Cu_2O has a cubic unit cell structure and an energy band gap of 1.7–2 eV depending on the deposition conditions[3]. The p-type conductivity is due to Cu vacancies in the Cu_2O. It is also a semiconductor with a direct forbidden gap, but some authors use the approach for direct allowed gap semiconductors in the case of Cu_2O, and as a result, widely different gap values were reported from 2.16 [4] to 2.5 eV [[5]. Since the band gap of Cu_2O is direct, the absorption coefficient of Cu_2O is relatively high (~105 cm^{-1}) and is comparable to some organic semiconductors. But still it gives non-satisfactory efficiency when implemented in a solar cell as an absorption layer due to its poor electrical property (remarkably high sheet resistance).

Properties of CuO. Another name for cupric oxide is tenorite and the crystal symmetry is monoclinic which is shown in figure 1.2. The crystallographic properties of CuO are listed in table 1.2.

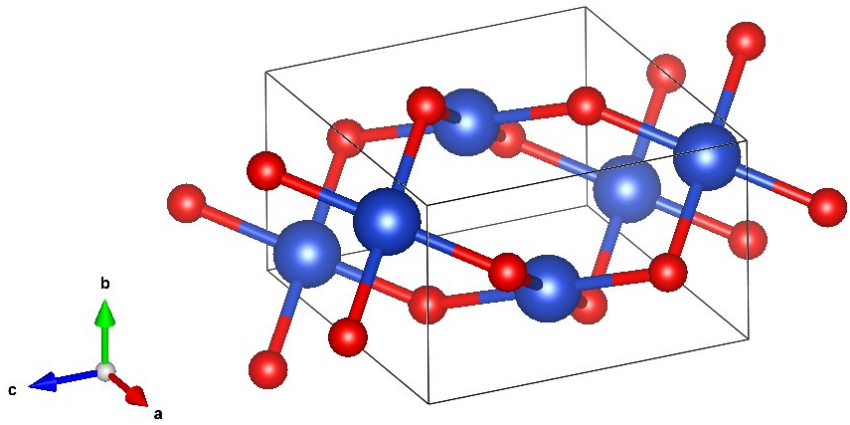

Figure 1.2. Crystal structure of the unit cell of CuO [2]

Table 1.2. Crystallographic properties of CuO [6]

Parameter	Standard value
space group	C2/c (No. 15)
Unit cell	a = 4.6837 Å
	b = 3.4226 Å
	c = 5.1288 Å
	ß = 99.548°
	α, γ = 90°
cell volume	81.08 $Å^3$
cell content	4 [CuO]
Formula weight	79.57
density	6.515 gcm^{-3}
distances	
Cu–O	1.96 Å
O–O	2.62 Å
Cu–Cu	2.90 Å
melting point	1201°C

Relatively little is known about the material properties of CuO. It has an indirect energy band gap of ~1.5 eV (in general), and the absorption coefficient is also high[3]. Since for a single p-n junction solar cell, the optimum band gap is 1.4 eV, the optical properties of CuO make it a very suitable semiconductor absorber material for solar cell applications[7]. In addition, the electrical properties of CuO such as majority carrier mobility and minority carrier diffusion length are also adequate.

Solar Cell

Solar cells are basically semiconductor p-n junction diodes which consists of mainly 2 layers, a thinner p-type semiconductor, and a thicker n-type semiconductor. This is mainly an electrical device which can convert light into electricity. To conduct the electricity, there are some metal electrodes constructed at the top of the solar cell, and the bottom has a metal layer as well for collecting the current. The entire cell has a glass/ ITO layer at the top for preventing reflection or mechanical shock.

The p-n junctions are formed as thin film, so that the uniformity of the film can maximize the absorption. When sunlight incidents on the top layer, the photons pass through that layer and reach the p-type semiconductor layer. As this layer is particularly thin, due to semiconducting effect, the photons reach the junction area, and the separation of charge carriers occur. The electrons from the depletion region pass on the negative side of the region which eventually pass current when connected to an external circuit.

The main factors controlling the efficiency of a solar cell are- shunt resistance, open circuit voltage, closed circuit current, and fill factor. These factors largely depend on various

other factors like transmittance (optical), electrical conductivity of the layer, band gap of the material, carrier concentration, and carrier mobility.

An Absorption Layer

The p type semiconductor layer in the junction is referred as the absorption layer or the active layer. The absorption coefficient, band gap energy, indirect/direct optical band gap, minority and majority carrier transport properties are major characteristics of a material in order to decide on its viability as potential for absorption layer. While incorporating the absorption layer with the window layer (n-type semiconductor) in the junction as thin films, the main challenges are lattice mismatch, spikes or cliffs in the conduction or valence band, band offset due to incorrect band alignment and so on. To address these challenges, research on prospective materials for absorption layer is necessary.

Working Principle of Absorption Layer

Absorber layer in a solar cell absorbs light passed through the glass layer from sun and gives rise to free electrons and holes in the junction. When an external electric field is applied, these free charge carriers (electron or hole) diffuse through the junction and drifts toward the transport layer (holes drifts toward the hole transport layer while electrons drift toward the electron transport layer). These drifted electron or holes are collected by respective metallic contacts or electrodes where the electrons dissipate energy and flows toward the opposite electrode to recombine with the holes at the junction again. The energy collected at the metal contacts produces power through the circuit. To prevent electron -hole recombination, electrons are needed to be extracted at the electron transport layer.

CuO And Cu_2O as an Absorption Layer

Researchers are now focusing on innovating nontoxic, low-cost, sustainable, and eco-friendly inorganic absorber layer material with application potential for solar electricity. Commercially adapted material for the absorption layer is silicon. But actual production of solar cells is facing some drawbacks for choosing this material. Thin Si films do not absorb solar energy well and the efficiency is much lower than the bulk version. Thin Si films do not absorb solar energy well, especially at sunlight's longer wavelengths in the 600–800 nm range. Improving absorption efficiency is thus a crucial part of designing efficient thin-film Si solar cells. Instead, transition metal oxides are used for transparent semiconductors for solar cell applications. Copper being a transition material, the oxides of copper are a potential candidate in this aspect.

Sustainability is another main reason for the steady interest in copper oxides for PV. Copper and oxygen are abundant elements such as silicon, so in the long run there can be no supply problem. This is one of the crucial requirements for a semiconductor to be used for large-scale PV power generation. As discussed extensively in [[8] conducted a careful sustainability analysis of a large number of semiconductor materials showed that Cu_2O and CuO are sustainable PV materials. In addition, all three oxides of copper are non-toxic and can be deposited as thin films relatively simply at low cost.

Cu_2O as an Absorption Layer. All three forms of copper oxides are semiconductors, and Cu2O is one of the first semiconductors studied for device applications.

The first published report of Cu_2O heterojunction solar cells with this structure was that by Herion *et al.* in 1980[9]. During the 1970s, there was a resurgence of interest in Cu_2O as a semiconductor for photovoltaics (PV) because of the need to develop terrestrial PV devices for

solar energy conversion in response to. The oil crisis in 1973 made researchers think of an alternative renewable source which led to the investigation of Cu_2O solar cells. The pioneer Cu_2O PV devices had Schottky Junction. After multiple attempts with various techniques, chemical reduction of the Cu_2O surface to Cu during sputter deposition was able to yield the best η 6.1% regardless of the metal deposited [[10]. A review of the literature on Cu_2O Schottky junction devices [[11] also pointed the low efficiency of solar cell using Cu_2O. Until 2006, the η of CuO heterojunction solar cells reported in the literature remained under 2%. The first report of a Cu2O heterojunction solar cell with an η above 3% was reported by the Kanazawa Institute of Technology in 2011. a polycrystalline Cu_2O substrate and absorber was first formed from Cu by using a three steps oxidation process[12] a η value of 6% was reported for a heterojunction PV device based on Cu2O and another metal oxide. An approach for the Cu2O heterojunction devices used pulsed laser deposition of an alloy on thermal Cu2O doped with a metal which was able to give efficiency of a value of 6.1%. Following that outcome, more research was conducted in this aspect and nowadays heterojunction devices are fabricated using PLD are demonstrating highest performances [13]

The Cu_2O PV research in this recent period is concerned with a search for newer dopants for Cu_2O, suitable transparent n-type semiconductors for heterojunction formation and low damage junction formation techniques which indicated improvements in the reported η of Cu_2O PV devices.

CuO As an Absorption Layer. Although, the narrower band gap of CuO is a better match to the solar spectrum compared with Cu_2O, little research on CuO heterojunction solar cells has been published until recently. The highest reported η as of 2015 for a CuO based PV device is 1.2%. A few works on particular association of phase mixture of copper oxide nano

powder were conducted, and one of them provided A high η of 2.88% for CuO heterojunction solar cell. The process of annealing and surface defect passivation were applied to CuO/ Cu2O heterojunction solar cells, and the fabrication process was changed to electrodeposition and electrochemical doping which showed a maximum efficiency of 0.64% as a result.

Limitations of Previous Work

Limitations of Cu2O Solar Cells. This article[12] highlights the susceptibility of the Cu_2O surface to solid state reaction, and hence the need to choose a low energy, low damage deposition method to form a true semiconductor heterojunction with Cu_2O. In the work of Akimoto *et al*[14], the sequence of deposition was found to have a major influence on the photovoltaic properties of the heterojunction fabrication. For the glass/Au/p-Cu O/i-ZnO/n-ZnO glass/Au/p- Cu2O /i-ZnO/n-ZnO (Cu2O first) structure, the reverse leakage current was relatively high, and a photovoltaic effect was high and a photovoltaic effect was almost unobservable. On the other hand, the glass/n-ZnO/i-ZnO/p-CuO (ZnO first) structure glass/n-ZnO/i-ZnO/p- Cu_2O (ZnO first) structure showed much better rectification and an η of 0.4% was obtained. The difference between the two was obtained. The difference between the two device structures was attributed to the similar atomic arrangements in the crystal structures of ZnO and the Cu2O for the ZnO first structure, which results in fewer interface defects. However, both V results in fewer interface defects but V_{oc} and short circuit current density, J became low because of these defects. It was observed that Cu2O works better as a substrate than as a layer in solar cells [15].

Limitations Of CuO Solar Cell. In 2012, a p-CuO/n-Si heterojunction solar cell fabricated by the reactive magnetron sputtering technique was reported [16]. Both V_{oc} and FF

were low because the high series resistance of the nanocrystalline CuO layer, and defects at the p-CuO/n-Si interface resulted in carrier recombination. The very thin CuO layer (100 nm) and the Cu grid top electrode might have also limited the amount of light absorbed by this device structure. A heterostructure study of Al/Ti/n-Si/p-CuO/Ti/Al by[17] found the CuO as a Cu rich copper oxide and a presence of amorphous interfacial layer (IL) due to residual oxygen in the sputtering system from the Raman data. Both parameters are detrimental to interface quality and thus need to be minimized by controlling the sputtering conditions of the CuO. They figured out that the increment of open circuit voltage is inversely proportional to the thickness of this interfacial layer and linearly proportional to the crystallinity of the CuO, and concluded that CuO deposition and annealing conditions play a crucial role in determining the achievable photovoltaic performance of p-CuO/n-Si heterojunction solar cells and the poor photovoltaic performance of p-CuO/n-Si heterojunction solar cells were attributed to native oxide formation and a Cu rich IL during the sputtering process.

The CuO film properties are influenced strongly by both the working pressure and annealing time. the CuO phase was found to have improved crystallinity when a higher working pressure was used. In addition, when annealed for a prolonged period, there is a phase transformation from CuO to Cu_2O and a mixture of CuO and Cu_2O was formed as a result. When the two-step process is used instead with the CuO layer deposited at higher power and doped with nitrogen, an η of 1.21% was obtained by[18], but it was also acknowledged that high sheet resistance and low carrier concentration of a CuO absorber layer are possible reasons of poor photovoltaic performance of copper oxide solar cells.

Research Objectives

A thin film of the phase mixture of copper oxide can be a lucrative material with good optical and electrical properties and attracts significant PV research interest due to interesting optical and electrical properties. The availability of composite elements makes the deposition of the thin film of the phase mixture economical as well. Thin film solar cells use lesser active material than bulk and so are cheaper. This is one of the reasons for solar cell industry to focus on heterojunction thin film solar cell. The research objectives can be divided into three parts. (a) synthesis of copper oxide phase mixture in bulk and finding the optimum parameters for the tuning, (b) synthesis of copper oxide phase mixture thin films using PLD technique and characterization to find a phase mixture of copper oxide with a balanced absorption and electrical property for the absorbing layer; and c) computational study of the phase transition of copper oxide by introducing oxygen vacancy using DFT. Accomplishment of these goals can avail the use this phase mixture of copper oxide in actual solar cells as an active layer which can offer a boost in the efficiency and can be a good option for commercial use.

EXPERIMENTAL METHODS

Chemical Methods

Sol-Gel Process. is a method which produces solid materials using small molecules as seed material. This is an affordable approach to fine control of the chemical composition of the product with a low temperature requirement. Even small quantities of dopants can be introduced in the sol and end up uniformly dispersed in the final product. It can be used in processing and manufacturing ceramics or as a means of producing very thin films of metal oxides for various purposes. Sol–gel derived materials have diverse applications in materials science.

This method is used for achieving extremely high levels of chemical homogeneity in colloidal gels. That is the reason it is used to fabricate metal oxides, and so in this experiment it was used to synthesize copper oxide. In this chemical procedure, a "sol" (a colloidal solution) is formed that then gradually evolves towards the formation of a gel-like diphasic system containing both a liquid phase and solid phase whose morphologies range from discrete particles to continuous polymer networks. In the case of the colloid, the volume fraction of particles (or particle density) may be so low that a significant amount of fluid may need to be removed initially for the gel-like properties to be recognized. This can be accomplished in any number of ways. The simplest method is to allow time for sedimentation to occur, and then pour off the remaining liquid. The general mechanism of the process is shown in figure 2.1.

Aging of a gel, a crucial step, also called syneresis, involves maintaining the cast object for a period of time, hours to days, completely immersed in liquid. After aging, Centrifugation was used to accelerate the phase separation process. Removal of the remaining liquid (solvent)

phase requires a drying process, which is typically accompanied by a significant amount of shrinkage and densification. However, this experiment did not require this step.

The produced gel can be used in mainly two ways. can be either deposited on a substrate to form a film (e.g., by dip-coating or spin coating), cast into a suitable container with the desired shape (e.g., to obtain monolithic ceramics, glasses, fibers, membranes, aerogels), or used to synthesize powders (e.g., microspheres, nanospheres). In this case, the produced gel was used to produce bulk CuO by air annealing.

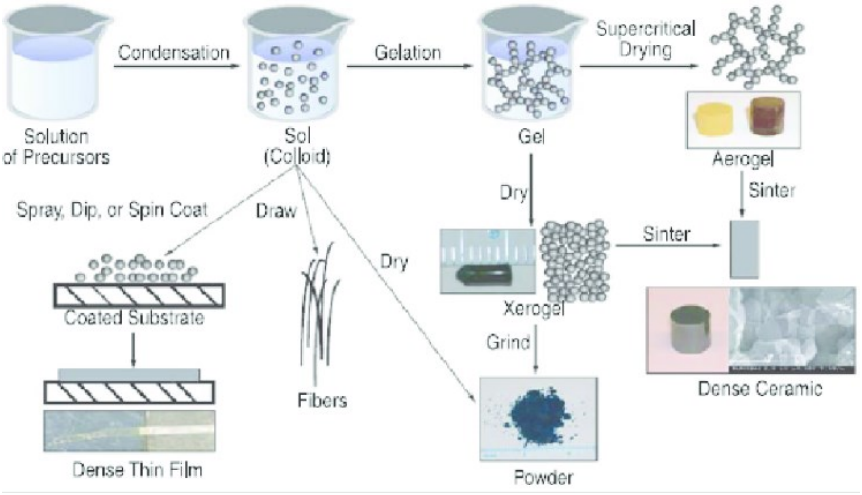

Figure 2.1. Sol gel process [19]

Drop Casting. is the formation of a thin solid film by dropping a solution onto a flat surface followed by evaporation of the solution as shown in figure 2.2.This method is easy to operate and can easily prepare a thick film, but this procedure is not convenient to produce uniform thin film. This method is used for the formation of small coatings on small surfaces. It requires a very small amount of solvent. Multiple droplets formed using this method provide a

distinctive environment to control the shrinkage direction and the evaporation rate of the droplets (Liu et al., 2014). In this method, solution is poured onto the substrate as drops and is allowed to dry without any spreading. When the droplets are projected onto the substrate, the liquid first spreads on the surface from the drop locations, due to the interfacial forces that are inclined to drive the droplet outward. As multiple droplets have been cast onto the substrate surface, when the edges of the droplet come in contact with each other, they mix together, forming a noncircular drop with the concave contact line. The schematic of the drop casting method is shown in Figure 2.5. The drop casting method is an alternative technique for polymer semiconductors, which are expensive and have poor solubility.

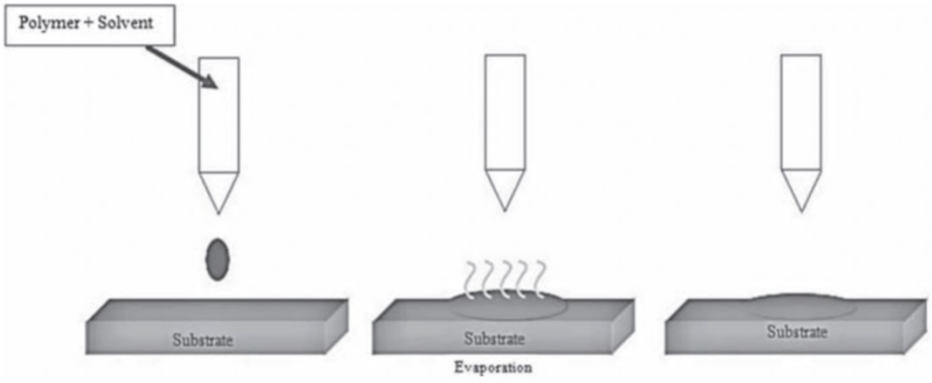

Figure 2.2. Drop casting method

Pulsed Laser Deposition

PLD is a very useful synthesis technique. This process is used to deposit thin films on various substrates. The deposited thin films are especially oxides. In this process, pulse from a laser source (situated outside of the reaction chamber) is used to supply energy. The unique technique provides the option of creating ultra-high vacuum inside the chamber and deposition in that controlled environment in presence of process gas. Another advantage of this process is that

stoichiometry of the material remains unaffected which gives the opportunity to grow thin films of oxides or metals or even superconductors at high temperature. Using multiple deposition even multilayers can be grown without harming the physical properties of each layer. The synchronized nature of this technique also accelerates the growth of multilayers. Moreover, different kind of gases can be used to tune properties like texture, magnetic properties, strain in thin films [20]

In the process of PLD, the laser beam is directed to the inside of the chamber hitting the target using one or multiple mirrors. When the laser hits the target, due to the energy from the laser shot the target surface ejects a vapor phase. Depending on various parameters this phase can be comprised of electrons, ions, molecules, and atoms in various ratio. The defining parameters for this ratio are energy density, vacuum pressure, wavelength, the pulse width of the laser, and gas pressure while deposition. This vapor phase forms a plume which can condense on a substrate at a specific rate depending on the surface energy. The full process occurs mainly in three steps [21]

a) The laser interacts with the target

b) plume of the target material forms and expands

c) the plume is deposited uniformly on the substrate inside the chamber with time.

Due to the interaction between the laser beam and the target, the electronic distribution of the target initiated to the excited mode which instantly leads to the uprise of the temperature of electrons which causes the vaporization of the target. As a result, the lattice is heated and generates plume [22]. Thermodynamics of the surface energy of the film and substrate dominates the energy of the interface and the characteristics of the film. But it also initiates the formulation of particles which is a huge drawback for the uniformity of the film sometimes [22]

For this experiment purpose a PLD set up, shown in Figure 2.3, with KrF (248 nm) laser source, 20 ns laser width, 325 mJ laser energy, and O_2 as the process gas was used.

Figure 2.3: Picture of the PLD set up for experiment in the lab

Parameter Analyzer For 2 Probe R Measurement

For the two-probe resistance measurement the Model 4200A-SCS Parameter Analyzer was used. This device can perform laboratory-grade DC I-V, C-V, and pulse device characterization, real-time plotting, and analysis with high precision and sub fA resolution. It includes a complete embedded computer. Its touchscreen interface accelerates and simplifies the process of taking data. It can generate I-V curve for any device connected in the circuit. The connection for I-V measurement of a resistor is shown in figure 2.4.

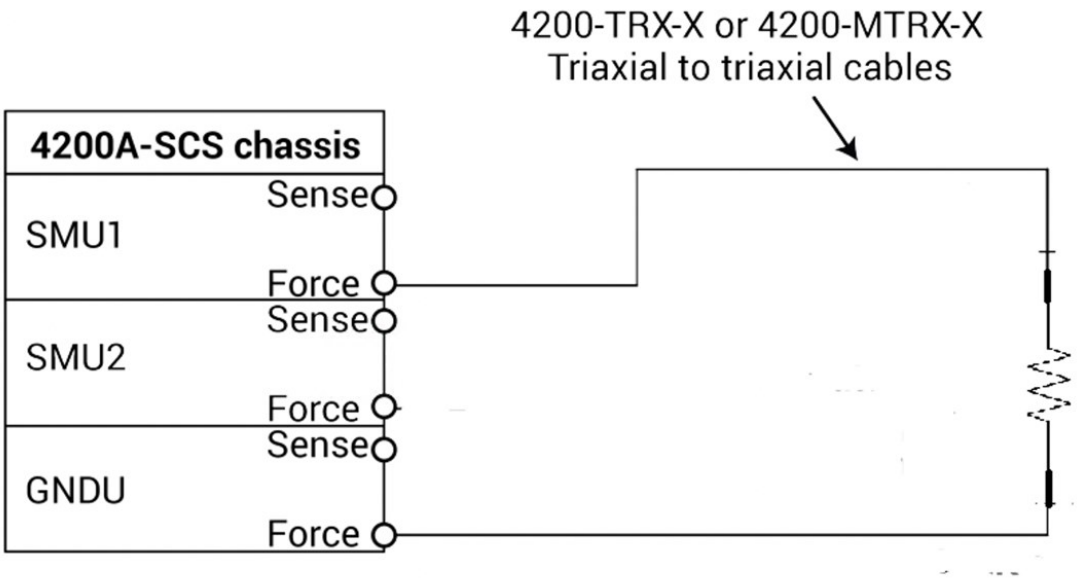

Figure 2.4. Connection for I-V curve of a resistor with the 4200-SCS parameter analyzer[23]

After the connection is done, a new project needs to be selected from the library and renamed according to the function of the project. Then the device needs to be connected and configured on the screen. While the configuration for ground is straight forward, the mode is set in SMU2 as shown in figure 2.5. The compliance needs to be set according to the range of the resistance. If the resistance is too high, the compliance needs to be set at low value to get the I-V curve. After the set up the result can be viewed and analyzed on the screen. The setup of the two probe R measurement station and the Parameter Analyzer 4200 is shown in figure 2.6.

Ac Measurement Setup

This process uses a function generator, an oscilloscope, a current amplifier, and LabVIEW (Laboratory virtual instrument engineering workbench). The LABVIEW program is written to measure AC current-voltage characteristics in dark and in light conditions. The

program was connected with a function generator, an oscilloscope, and Keithley 617 programmable electrometer using GPIB.

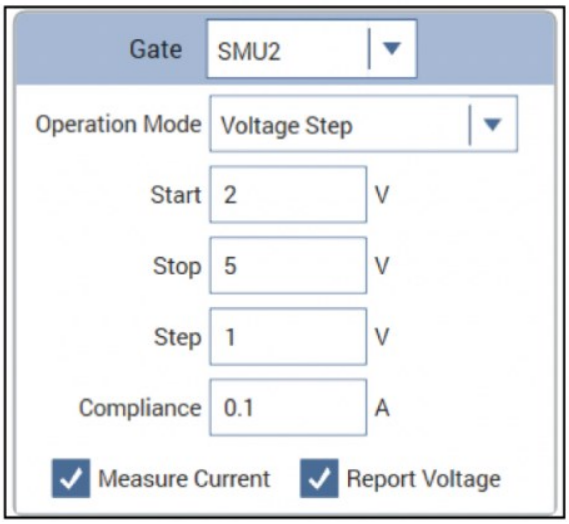

Figure 2.5. Configuration for SMU2 [23]

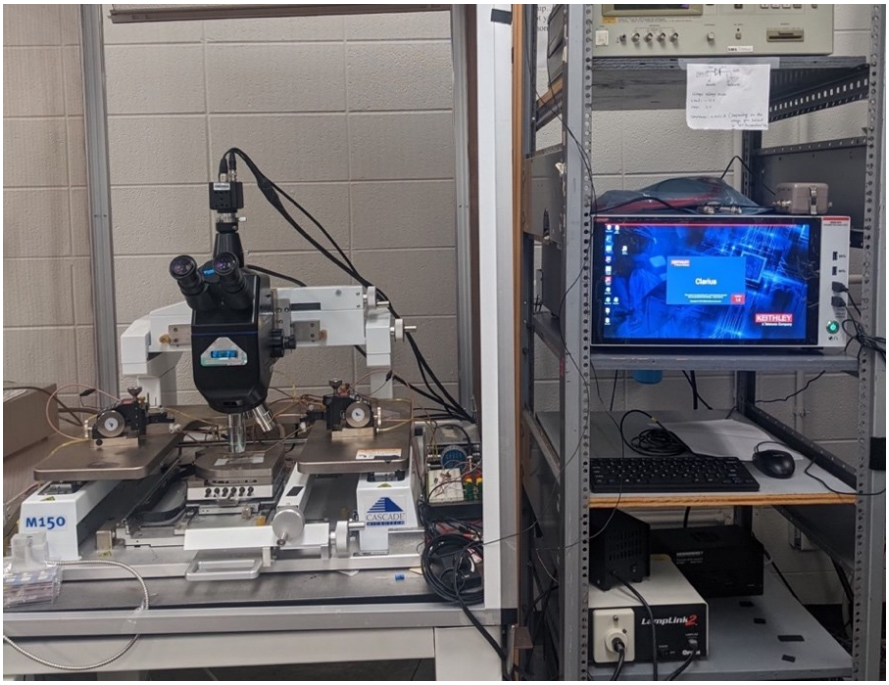

Figure 2.6. The lab set up of the two probe R measurement station and the Parameter Analyzer 4200

UV-VIS For the Measurement of Transmittance

The amount of absorption for a material depends linearly on the concentration of the molecules with absorbing ability in the material. This relation was expressed mathematically by Beer-Lambert as, $\log (I_0/I) = \varepsilon lc$; [24]

Here,

ε = absorption coefficient,

l = the length of the absorbing material

I_0 = the intensity of the incident radiation,

I = the intensity of the transmitted radiation, and

c = the concentration of the molecules with absorbing ability.

Due to absorption in the material, the outermost electrons of molecules are excited and transits from ground state to excited state depending on either pi and sigma electrons or charge transfer electrons or the electrons in the d and f bands [24].

When the transition of electrons occurs to the excited states, electronic energy level is formed consisting of both vibrational and rotational energy level at top of it with their individuality. This causes the absorption spectra to broaden, and absorption peaks appear as a result. Electronic and vibrational energy level of a material is shown in a Figure 2.7. Different types of electronic excitations in materials are demonstrated using UV-vis shown in Figure 2.8 uses HR4000 high-resolution miniature fiber optic spectrometer with 0.025 nm (FWHM) resolution and 200-1100 nm spectral range to collect UV-visible spectra. The spectral range can be varied by changing entrance slits and grating. The fibers used for this entire operation is and the connection between the spectrometer and any desktop (to visualize) is provided using universal serial bus. To collect data points for the overall spectra, ocean optics

software is used.

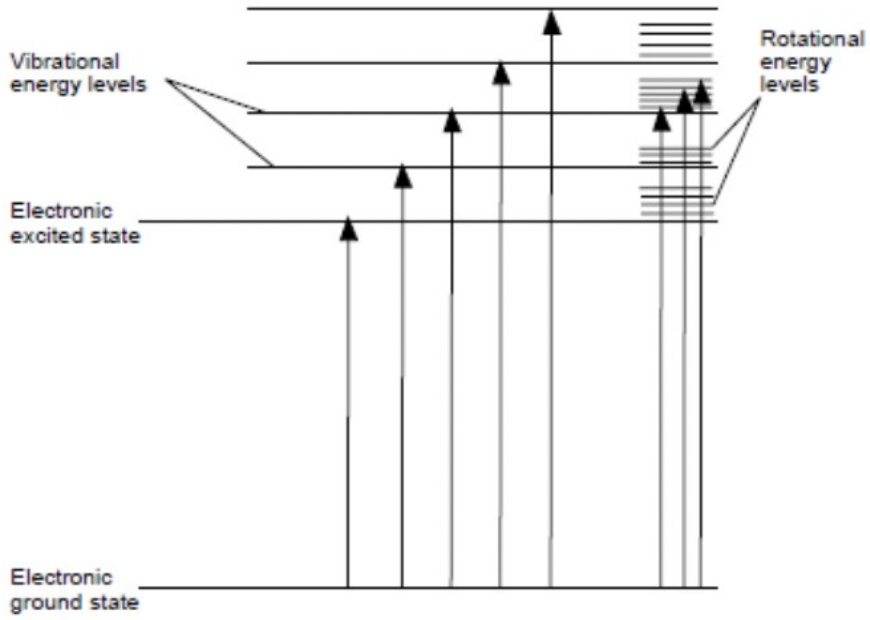

Figure 2.7. Levels of vibrational and electronic energy [24]

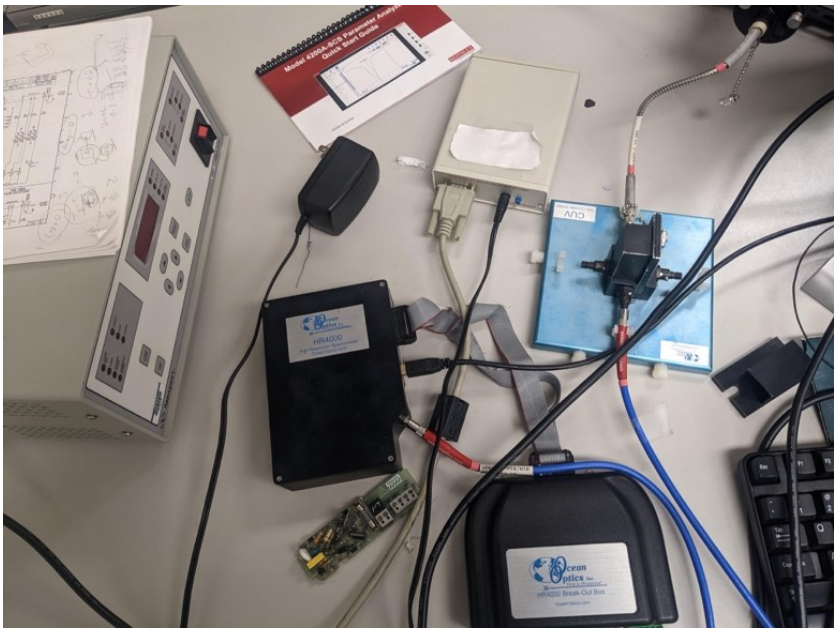

Figure 2.8. UV-VIS set up used for the experiment

X-Ray Diffraction Structural Study

XRD (X-Ray Diffraction) is mainly used to observe the crystalline structure of any compound at atomic level. As every single crystal appears with its own unique structure, it shows its individual crystallographic pattern in XRD. So, by observing the pattern for any compound in XRD, the crystal structure for that specific composition can be easily detected. Not only the crystal structure but the bond angles and lengths, strain between each bond, preferential oriented planes (if any present), and other characteristic properties for that composition can also be extracted from the XRD pattern. XRD is an important tool in materials science because of its versatile nature in demonstrating crystal structure. Diffraction for x-ray can only be found when x-ray hits onto a crystal structure with periodicity in its structure. There is an occurrence of the scattered electromagnetic waves. When high energy x-ray beam encounters crystal structures, constructive and destructive interference occur resulting in diffraction and appearance of peaks [25].

The lab set up shown in Figure 2.9 includes a Bruker D8 Discover X-ray diffractometer which has been used to collect XRD patterns of bulk and thin films synthesized in this work. The components of the XRD machine used are:

a) X-ray source

b) Incident beam optics

c) Goniometer (X, Y, Z, phi, chi scans), and

d) Area detector

Diffrac plus Topas software is used for peak profile analysis and EVA (evaluation) software does the plotting.

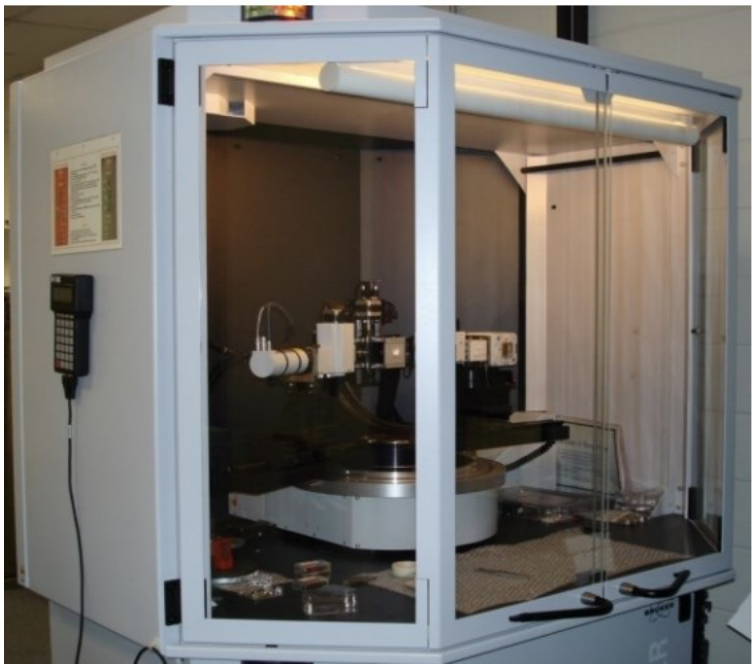

Figure 2.9. The set up for XRD machine used in the lab

Raman spectroscopy

When any monochromatic radiation incidents on a material, it undergoes scattering depending on the frequency of the radiation relevant to the frequency of the material and labeled as Rayleigh or Raman scattering. If the scattering involves no change in energy, it is labeled as Rayleigh, whereas the ones involving a change in energy is labeled as Raman scattering. The collective scattered radiation with new frequencies is referred as Raman spectra. Raman scattering can be divided into two types of namely Stokes scattering and Anti-stokes scattering. Radiations involving reduced vibrational frequency ($\omega 1-\omega m$) are termed as Stokes scattering and scattered radiations with increased vibrational frequency ($\omega 1+\omega m$) are referred as anti-stokes scattering. The Horiba Labram PL-Raman system shown in Figure 2.10. is used for Raman spectroscopy. There are total three lasers for different purposes (green, red, and blue with different

wavelength). The Green laser (532 nm) and red laser (785 nm) are mainly used to determine the Raman active materials.

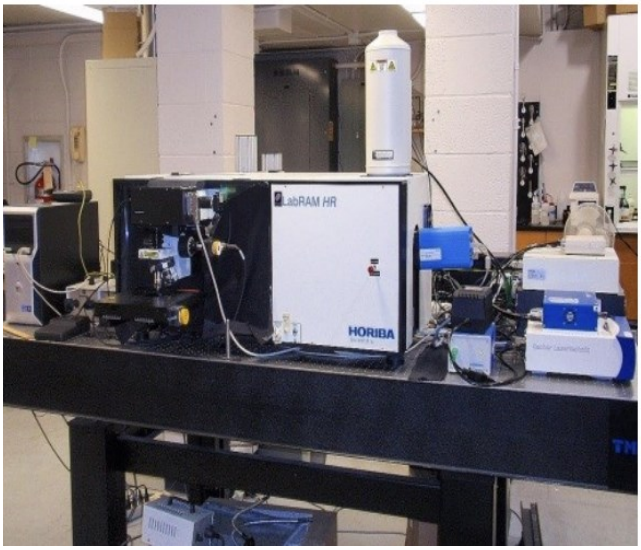

Figure 2.10. The set up for the Raman-PL spectroscopy

SEM & EDS Set Up

SEM (Scanning Electron microscopy) is a system to observe morphology of any specimen which consists of a) an electron gun to shoot the electron beam, b) specimen stage to put the specimen steadily, c) electromagnetic lens to focus, d) secondary electron detector to detect the secondary electrons emitted from the material; and e) high vacuum system to ensure controlled system. The details of the scattered electron by a specimen are comprehended using Monte Carlo simulations. SEM radiates electron beams onto the surface of a specimen to observe the morphology. The randomly scattered electrons are dependent on the atomic mass and atomic density of the material. This radiation initiates the emission of secondary electrons from the material and a secondary electron detector are used to collect these secondary electrons [26] The EDS can provide quantification of the elements present in the specimen and elemental mapping

along with point scan, line scan, or even area scan. The lab set up shown in Figure 2.11 uses a FEI Quanta 200 S FESEM to collect SEM images and EDS elemental scans.

Figure 2.11. The FESEM set up for the experiment

SYNTHESIS OF BULK COPPER OXIDES PHASE MIXTURE

Goal

The focus of this work is to use the phase mixture of copper oxide as a potential material for the active layer of a solar cell. First it is important to find out whether a stable phase mixture can be produced. To examine that, initially copper oxide was produced in the bulk form. Then it was experimented if the phase percentage of the two phases of copper oxide was possible to vary in a mixture. To vary the phase mixture mainly reduction annealing was used, and various approaches were experimented to adapt the best one for varying the phase mixture.

Motivation

Previous studies have experimented with the phase mixture of copper oxide, and they were able to produce mixed-phase copper oxide nano-powders (NP). They showed that the performance of CuO and Cu_2O heterojunction solar cells can be further enhanced using this NP. They hinted at the possibility of an in-between indirect band gap due to the phase mixture which may offer a boost in light absorption of the material. But they also faced some limitations which hindered the consideration of phase mixture of copper oxide as a potential material. This study tried to address those limitations and find alternate perspective.

Literature Review

Previous work [27]was able to construct a copper oxide based solar cell where they used phase mixture of copper oxides (nano- structured) with high optical activity. In their work they demonstrated the nanostructured phase mixture of copper oxide as a good potential material for

solar cell which can provide higher efficiency. Stability of NS was established through Raman spectroscopy and X-ray diffraction, and the NS exhibits a very large optical absorption coefficient of 7.05E+5 cm^{-1} at wavelength of 525 nm. which is appreciably larger than that of a pure standard CuO and Si. Their study also found a unique one-dimensional lassie nanostructure measuring less than 50 nm.

Limitations. The work in [27] was able to demonstrate impressive absorption property of the NP of the phase mixture of copper oxide and to incorporate it as an absorption layer in a solar cell. However, they faced some major limitations which can be the bottleneck for using this material as an option for farther implementation in solar cell. These major limitations are necessary to overcome to consider this phase mixture of copper oxide as a budding active material for solar cell application.

- One major drawback this study faced that electron mobility was greatly hampered by nano-powder. Due to the nanostructure, the films were non-uniform, and it shows high resistivity when it was incorporated in a solar cell as an absorption layer. As a result, electron mobility is too low in real devices
- This particular phase mixture was also difficult to recreate. Which made it inconvenient for considering as a regularly accepted alternate for use in solar cell.
- The unrepeatability and ambiguity on exact parameters made it strenuous to produce on a large scale.

To address these limitations, this thesis focused on

- microstructure instead of nanostructure to be able to provide a balance between high absorption coefficient and electron mobility.

- Different synthesis approaches to adapt the procedure which offers production on a large scale with low cost.
- Experiment on optimum parameters for better fine tuning and recreation.

Methodology

Sol Gel Method. is a versatile process used in making various ceramic materials. In a typical sol-gel process, a colloidal suspension, or a sol, is formed from the hydrolysis reactions of the precursors, which are usually inorganic metal salts or metal organic compounds such as metal alkoxides. The obtaining of metal oxides by the sol-gel method is the subject of much interest, in view of the simplicity, low cost, reliability, repeatability and relatively mild conditions of synthesis. In this study metal salt (CuSO4.5H2O) and strong base (NaOH) was used as precursors.

Drop Casting. Drop Casting is a simple process where a solution is dropped onto a substrate usually resulting in spread of the liquid solution and the formation of a non-uniform thin solid film after solvent evaporation. In this study, the gel of Cu(OH)2 produced by sol gel process was casted on a glass substrate placed on top of a hotplate using a dropper at 240° C.

Description of the Process. (0.15 M) $CuSO_4.5H_2O$ (GFS Chemicals) was dissolved in (20ml) deionized HPLC water (GFS Chemicals) under constant magnetic stirring. NaOH (2N) was added to the resulting solution which was aqueous in nature until the pH reached 12.2. The below mentioned reaction takes place:

$CuSO_4.5H_2O$ (aq.) + 2 NaOH (aq.) → Na_2SO_4 (aq) + $Cu(OH)_2$ (s) + 5 H_2O (l)

The product of this reaction was left for aging for 24 hours. The solid-liquid products were centrifuged using “LW Scientific centrifuge, Model E8” at a rotation speed of 1600 rpm for 3

times each having a duration of 20 min. Then the solution was washed three times with distilled water and ethyl alcohol to remove the ions possibly remaining in the final product until the pH level reached 7.5. Then the solution was drop-casted on a glass substrate at 240°C. After that the drop casted non-uniform film was air annealed at 600°C using a furnace for 3 hours. The end product was mostly cupric oxide (CuO) which was verified from the XRD data analyzed by TOPAS. The comparison of XRD data of the end product with the cif files for CuO, Cu_2O and Cu are shown in figure 3.1 which shows that the peaks of the end product match mostly with CuO phase.

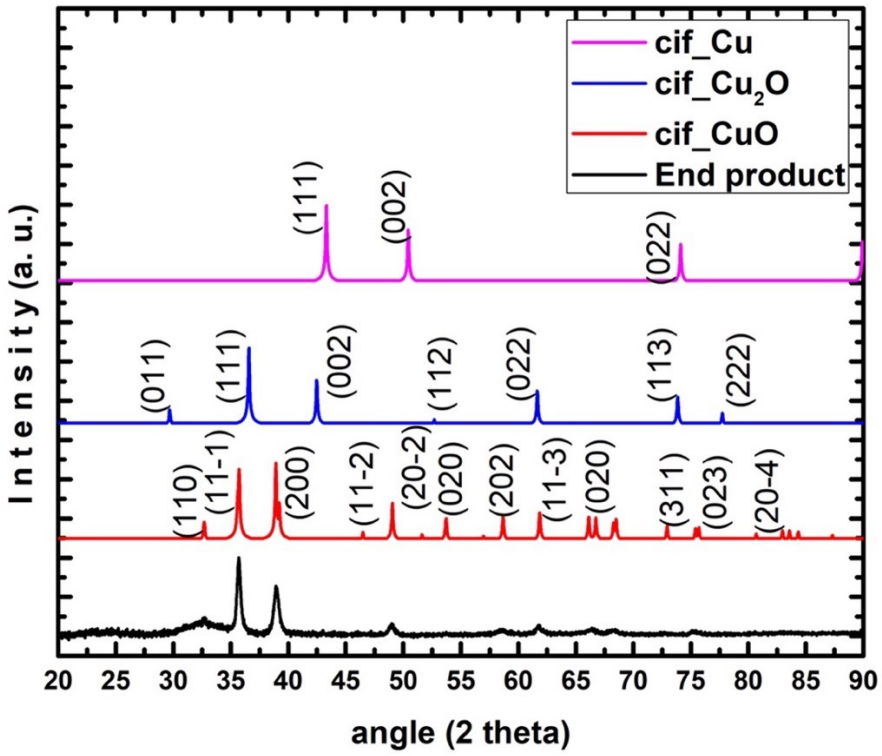

Figure 3.1. Comparison of the XRD data of the end product with the cif files of CuO, Cu_2O, and Cu

Reduction Annealing. In metallurgy and materials science, annealing is a heat treatment that alters the physical and sometimes chemical properties of a material. To make it more

feasible for experiment, annealing can reduce its hardness by increasing its ductility. In this process in a controlled sealed system, temperature is increased, decreased, and kept constant for certain time in one or multiple steps, each steps having a specific rate of increasing or decreasing temperature. Reduction annealing is the process where annealing takes place in a H_2/Ar gas atmosphere to create oxygen vacancy on the surface of a sample.

General Description of Hydrogen Reduction Annealing. After the air annealing of the drop casted sample, it was confirmed from the XRD data that the product is mostly CuO. To create phase mixture of copper oxides in this sample, hydrogen reduction annealing is used. After inserting the sample inside the furnace and sealing it from the outer atmosphere, vacuum was created using a turbo pump so that no air remains present inside. Then H_2/Ar gas was flown inside the furnace, and the annealing was conducted in the presence of the H_2/Ar gas. When the temperature is optimum, a few reactions might take place inside the furnace.

$$2H_2 + O_2 \Leftrightarrow 2H_2O \text{ [100°C]}$$

$$2CuO + H_2 \Leftrightarrow Cu_2O + H_2O$$

$$Cu_2O + H_2 \Leftrightarrow 2Cu + H_2O$$

Mechanism of reduction annealing: $CuO \rightarrow Cu_2O \rightarrow Cu$ [In presence of H_2/Ar gas at high temperature. Following the above-mentioned equation, the phase changes and we get mixture of various phases depending on the temperatures and duration of the annealing.

Optimum Parameters

During the process of annealing, there are three main parameters which play role as a deciding factor of the percentage of phase mixture.

Time. plays a crucial role in the process of annealing. As Cu_2O is an intermediate phase between CuO and Cu, longer annealing can easily convert the Cu_2O into Cu in presence of hydrogen. On the other hand, very little time in annealing can vary the rate of reaction which can result in variation in the phase percentage. Also, very little time to rise a very high temperature can cause quenching.

Pressure. is another crucial parameter in the annealing procedure. As it is the parameter directly affecting the annealing temperature. In this study, pressure was kept constant at 1.5 psi (overpressure to prevent the air from outside to enter the system) to see the effect of temperature in variance of the percentage of phase mixture.

Temperature. is the most crucial parameter in the process of annealing. If the temperature is too low, there might be no reaction. On the other hand, if the temperature is too high, it might introduce new unstable phases and mess with the crystal structure. For example, if the temperature is lower than 300°C, there might be no reaction at all even with a longer time. On the other hand, if the temperature is higher than 500°C, there is possibility of getting too much Cu in the sample.

For this experiment, the adapted strategy was to keep the pressure constant and vary parameter between the other two to see the effect of change on the phase percentage. So, at constant pressure, at first, the temperature of the reduction annealing was varied keeping the time for annealing constant. And when a suitable temperature was found, time was varied, keeping that temperature constant. That is how the time and pressure for creating different phase mixture were fine tuned for figuring out optimum temperature and time for reduction annealing.

Phase Mixture Variation Using Reduction Annealing in Various Ways

1st Approach. The 1st approach was to anneal the sample in PLD chamber at 500°C with constant flow of H_2/Ar gas. The used vacuum pressure was 2 mTorr and annealing pressure was 20.7 Torr. The outcome of this approach was not satisfactory. It had a trace of Cu which was inferred from the XRD data. So, this sample was not viable for solar cell applications.

2nd approach. Putting the sample in a tube furnace and seal it. Then at a constant pressure, flushing with Ar gas and then annealing in presence of H_2/Ar gas (reduction annealing). As an outcome, some changes were noticeable, but not as expected. There was not much change in the phase percentage and the sample contained mostly CuO. The probable reason can be the presence of more O_2 which is hindering the proper reduction of O_2. Later the system was identified the presence of leak.

3rd approach. The 3rd approach was to create vacuum by pumping, and constantly keeping an overpressure so that even if there is some leak, it doesn't let the O_2 from air get in, and the gas flows out instead. Then the sample was annealed in presence of H_2/Ar. This approach brought out a good result. There was a shift in the position of the peaks in XRD data, which is a confirmation on varying phase from XRD data.

The comparison between the output from all three approaches with the standard cif files are shown in figure 3.2. From the reduction annealing, the XRD data of various samples showed that higher temperatures like 500°C to 700°C causes too much reduction which leaves Cu in the sample. On the other hand, 200°C is below the temperature required for reaction. For 300°C it takes way longer time for the reaction to occur. 350°- 400°C is the optimum temperature range where the reaction is more spontaneous and systematic. As for time, it also depends on the temperature. For example, reduction annealing for 15 minutes at 500° C is causing almost no change while 700° C causing too much reduction and trace of Cu according to figure 3.3. When

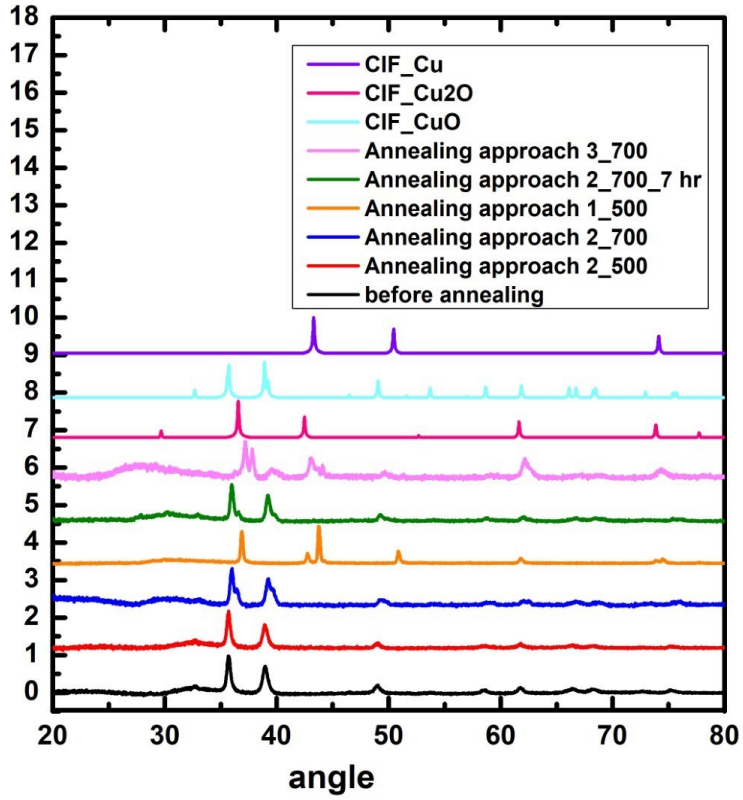

Figure 3.2. Comparison of the XRD data of samples annealed with different parameters and data generated from different cif files

a time duration of 1 hour was taken as standard, 400° C gave the most convenient and systematic transition of phases, but it still had Cu in it which makes it non-convenient for being used in solar cell. So, a time duration of 30 minutes for the reduction annealing at 400° C can be optimum to have a balanced mixture of phases of copper oxide. And then varying time should be varying the percentage of phases in the mixture. However, similar parameters yielded little discrepancy in the result which can be attributed to non-ideal environment due to slight leak in the system.

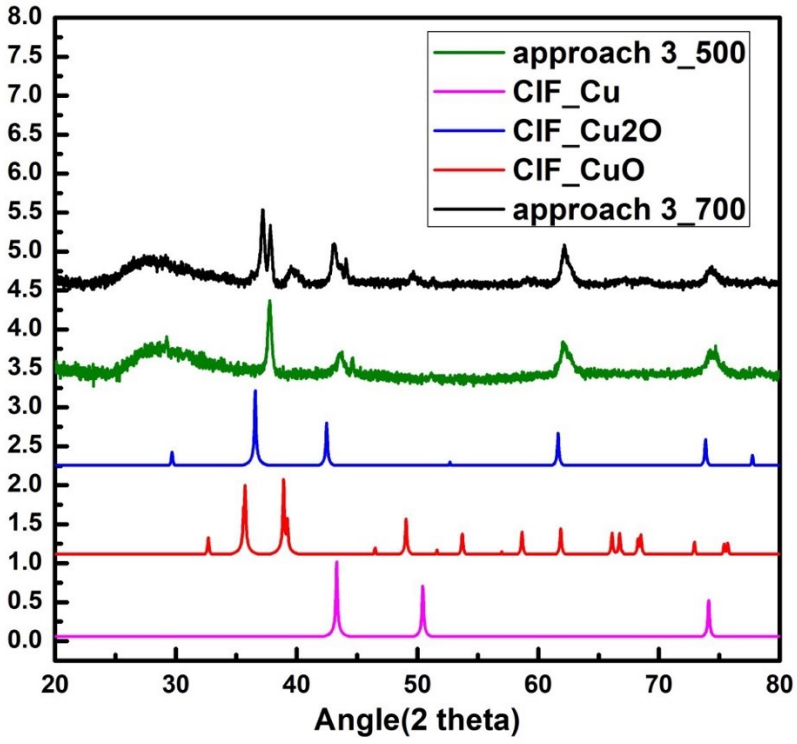

Figure 3.3. Comparison of the XRD data of outcome from approach 3 at 500°C and 700°C at constant annealing time (15 min) and data generated using cif files

Summary

• CuO was successfully reduced at 500°C and 400°C as shown in figure 3.4.

• Almost no reduction at 300°C, 1 hour according to figure 3.4. Longer time might have some reduction.

•Phase percentage was found from the Rietveld refinement of XRD-Data using TOPAS software.

• Annealing at 500°C, 1 hour reduces to Cu (38.46 wt.%)

• Annealing at 400°C, 1 hour reduces to Cu (24.69 wt.%)

• Excess amount of metal is not useful for solar cell application.

• Optimum temperature is in the range of 350°C- 400°C.

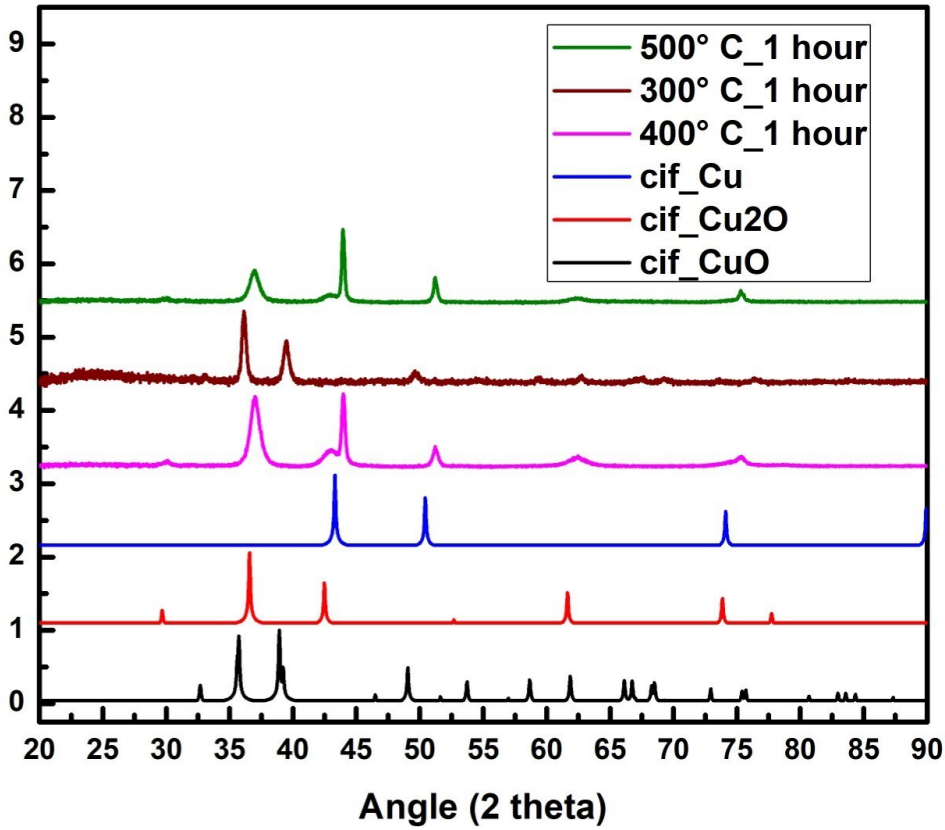

Figure 3.4. Comparison of the XRD data of outcome from approach 3 at 300°C, 400°C and 500°C at constant annealing time (1 hour) with the cif files

STRUCTURAL, OPTICAL, AND ELECTRICAL CHARACTERIZATION OF PHASE MIXTURE OF COPPER OXIDE THIN FILMS

X-ray Diffraction and Rietveld Analysis

Phase mixture copper oxide thin films were synthesized using PLD and X-Ray diffraction was used to do structural characterization of all the samples. Crystallographic Information Files (cif) of CuO, Cu_2O and Cu were collected from **Crystallographic Database** to match with the XRD analysis data from the samples which are shown in figure 4.1, 4.2.a) and 4.2.b) Figure 4.3 and 4.4 shows the Rietveld analysis of the XRD of 4 selected samples of thin films where the black lines are the experimental data, the red lines are the calculated data from Rietveld analysis, and the blue lines are the difference profile. Samples S1, S2, S3, and S4 represent phase mixture of copper oxides which were formed under varied reaction parameters in PLD and demonstrate different

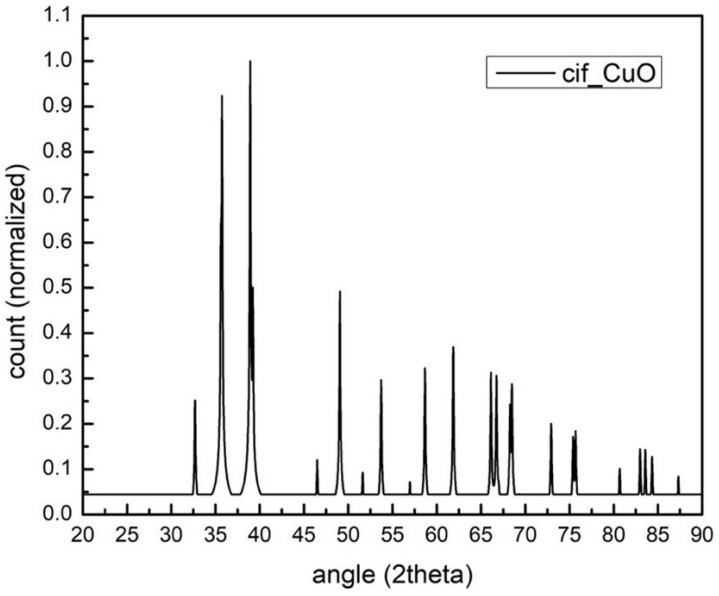

Figure 4.1. Crystallographic Information File for CuO

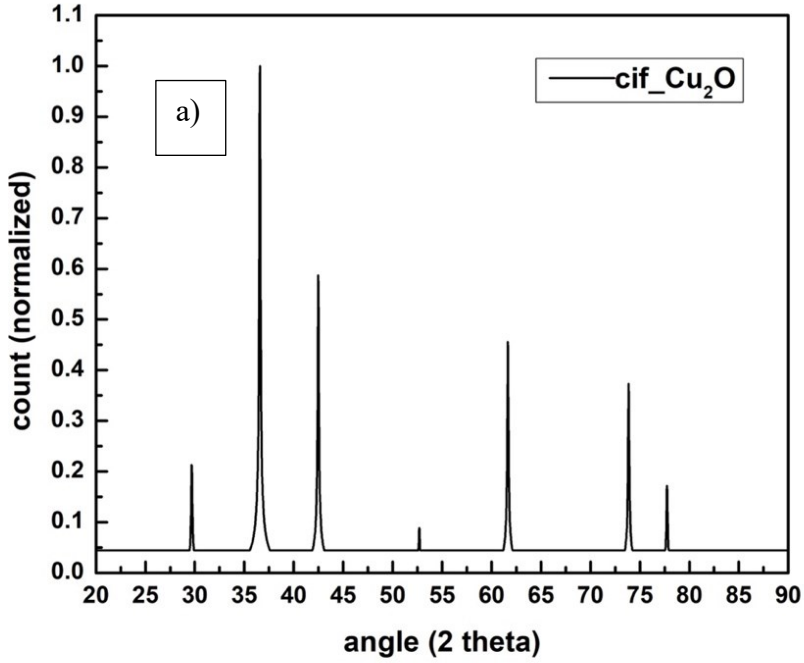

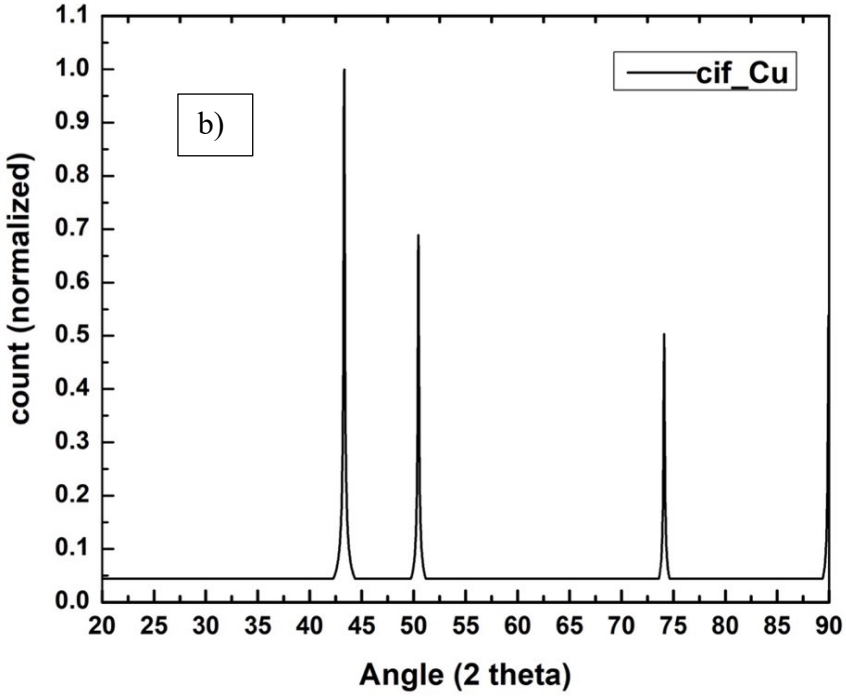

b)

Figure 4.2. Crystallographic Information File for a) Cu_2O and b) Cu

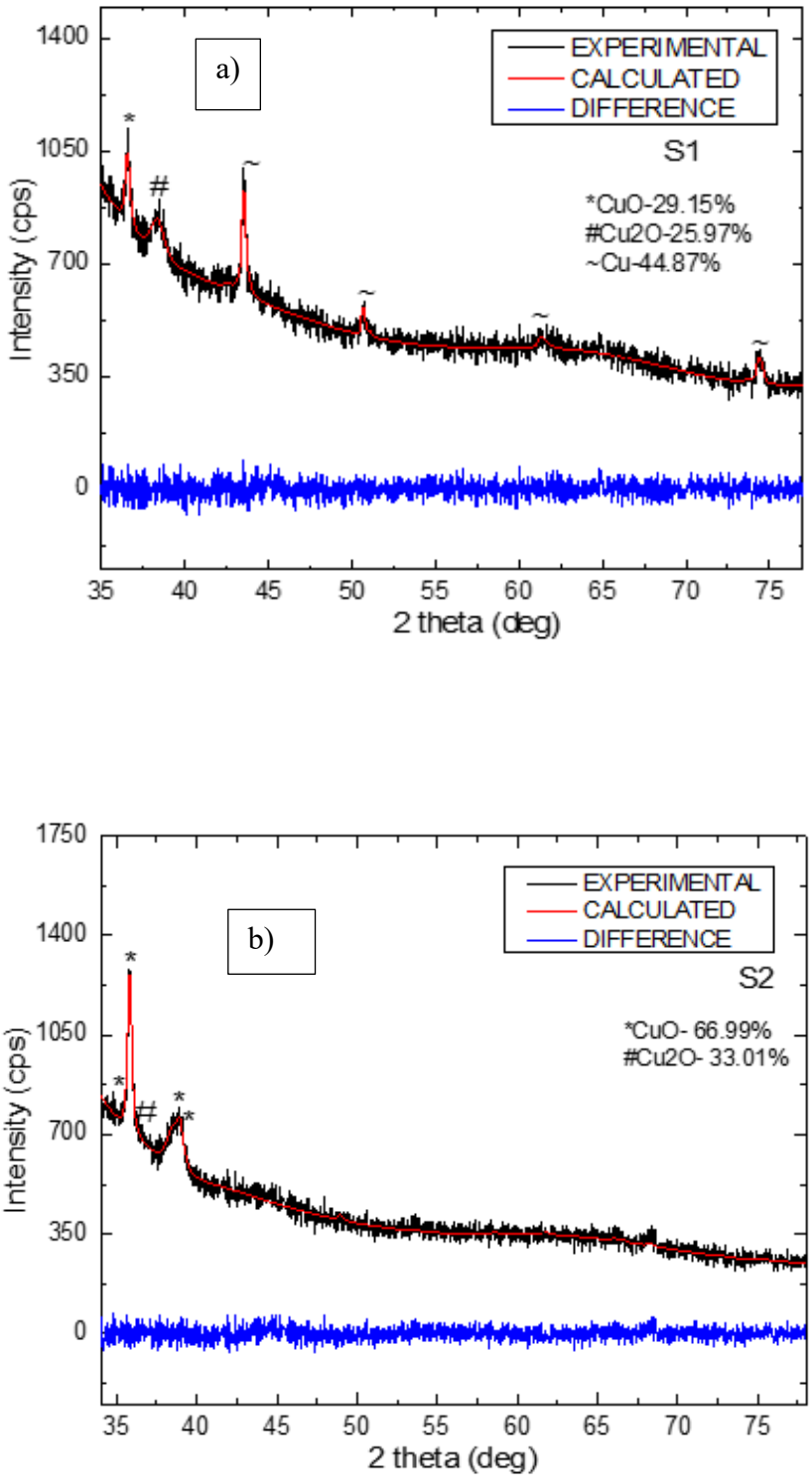

Figure 4.3. Rietveld fitted XRD pattern of a) S1 and b) S2

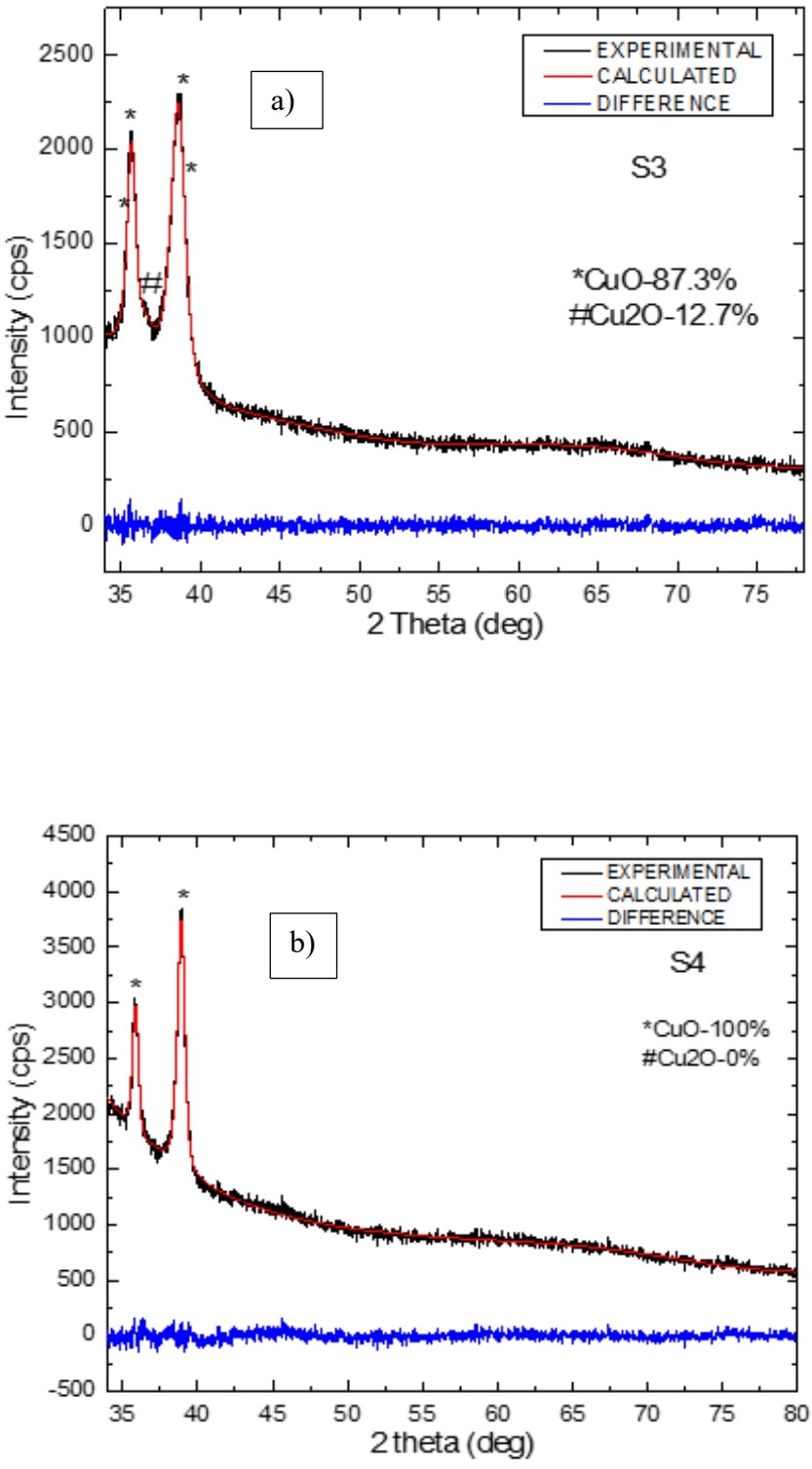

Figure 4.4. Rietveld fitted XRD pattern of a) S3 and b) S4

optical absorption and electrical characteristics. The analyzed data indicate the formation of CuO and Cu2O mixture which have crystallized in monoclinic with space group symmetry of c12/c1, and cubic with Pn3mZ symmetry, respectively.

In Figure 4.3. and 4.4. the black lines are the observed pattern where the red lines are calculated using Rietveld analysis, and the blue line shows the difference profile. From the Rietveld analysis, it is observed that the phase (weight) percentage is varying in the samples. Sample 1 has peak at 43.29, 50.47 & 74.12 which are coming from copper and 36.42 which is coming from cuprous oxide, and 38.38 which can be shifted peak of cupric oxide which is originally situated at 38.68 & 38.98. In sample S2 and S3, there are hints of convoluted peak from both CuO and Cu_2O. From the Rietveld analysis it can be said that sample 3 has sharper peaks for CuO than Cu_2O, and the percentage of CuO is higher than Cu_2O indeed. It has 87.30% of CuO and 12.7% of Cu_2O. From other characterizations, it is seen that this particular phase mixture has given good electrical and optical properties.

The analysis of XRD data indicates the preferential orientation of Cu2O toward (111) direction and CuO toward both (200) and (111) directions. In sample for the Rietveld Analysis indicated 100% of CuO and from the figure it is confirmed from the sharper and narrower peak at 35.5 and 38.98 which comes from CuO. While doing the structure property analysis, sample 4 is taken as the standard for comparison as pure CuO. The phase (weight) percentage of CuO and Cu2O in all 4 samples from the Rietveld analysis are provided in table 4.1. From the Rietveld analysis we see both the Gaussian and Lorentzian strain effect which is very little on each film. The GOF values for the TOPAS analysis are provided in table 4.1. to indicate the accuracy of each fitting. Sample S4 has 100% CuO. The bond length of (Cu–O) is 1.961 Å for pure CuO [28]

Table 4.1. The phase (weight) percentage of CuO and Cu_2O in the samples

Sample no.	CuO/ Cu_2O (%)	Goodness of fit (gof)
S1	CuO 29.15% Cu_2O 25.97% Cu 44.87%	1.06
S2	CuO 37.77% Cu_2O 62.23%	1.06
S3	CuO 87.30% Cu_2O 12.70%	1.09
S4	CuO 100% Cu_2O 0%	1.22

The annealing temperature, film thickness, and other defining parameters were kept constant. From the structural analysis it is observed that the change in the size and strain is random to have any systematic effect on the property. So, the only effective factor which can influence the absorption property is the difference in the percentage of the phase which is controlling the electrical and optical properties.

Optical Absorption

Absorption Coefficient. The absorption coefficient determines how far light of a particular wavelength can probe into a material before it is absorbed. In a material with a low absorption coefficient, light is only poorly absorbed, and it will appear transparent to that wavelength in case of thin material. Increase in optical absorption co-efficient indicates the possible increase in the efficiency of a solar cell when used as an absorption layer.
The equation used for the calculation of absorption coefficient is as followed:

$\alpha = (2.303/t) * (\log10 (A))$

Where, α= absorption coefficient;

t= thickness of the film;

A= 1/T(transmittance) = I_0 /I;

I= intensity of the light spectrum passing through film along with the glass

I_0 = intensity of the light spectrum passing through the glass substrate; Both the material and the wavelength of light play a role in determining the absorption coefficient. Semiconductor materials have a sharp absorption coefficient, since light which has energy below the band gap does not have sufficient energy to excite an electron into the conduction band from the valence band. Consequently, this light is not absorbed [29] In the absorption layer, electron-hole pairs are generated, and each carrier drifts separately according to the electrical field to p- and n-layers, then diffuses to electrodes, and finally comes out as the photocurrents.

In Figure 4.5. the transmitted intensity of 4 samples are shown. Glass used as a background. The pink line is the transmitted intensity for S3 which has the highest absorbance, and so the highest absorption co-efficient. The absorption coefficient of all samples is calculated in table 4.2.

Table 4.2. The absorption coefficient of the samples

Name of the sample	Absorption coefficient
S1	9.80E+4 cm^{-1}
S2	1.12E+5 cm^{-1}
S3	3.25E+5 cm^{-1}
S4	9.89E+4 cm^{-1}

According to the phase percentage calculated by the Rietveld Analysis, sample S5 has 100% CuO and the band gap from the indirect band gap calculation (as pure CuO has indirect BG) also matches with pure CuO which is 1.1 eV.

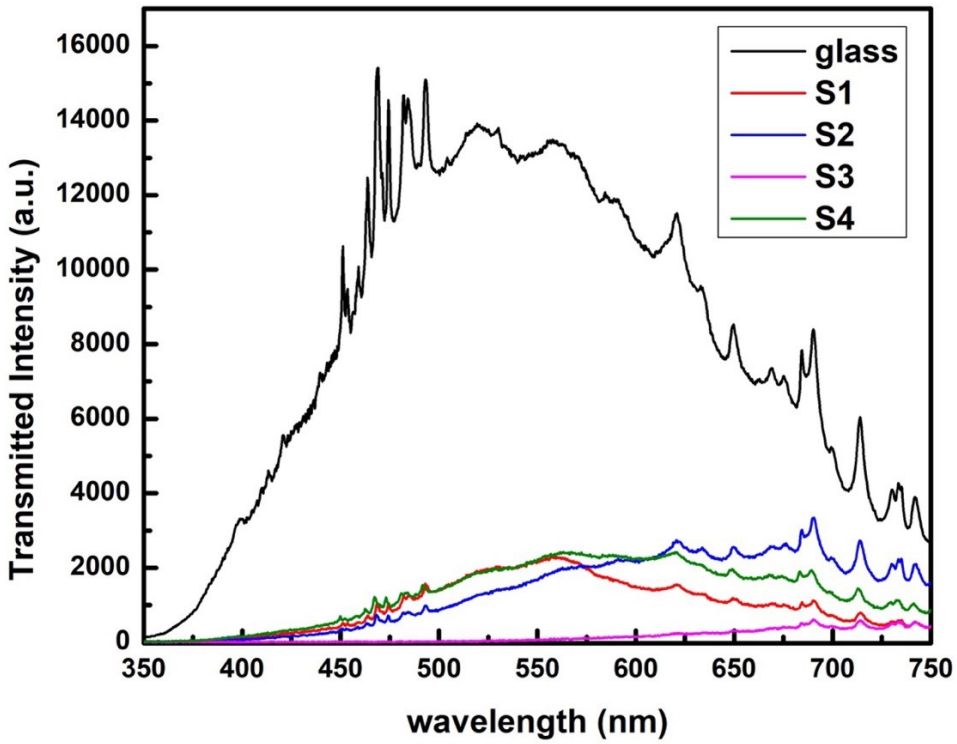

Figure 4.5. Solar transmitted intensity of the samples

In general, CuO thin films have a high absorbance in the visible spectrum (in the range of 10^5/cm), which decreases with increasing wavelength. From the table we can say that S2 and S3 which has phase mixtures of (CuO 37.77%, Cu_2O 62.23%) and (CuO 87.30%, Cu_2O 12.70%) respectively has high absorption co-efficient, and S3 has the highest absorption co-efficient. The high reflectance and low absorption (< 15 %) in S1 can be attributed to the presence of metallic Cu. S4 has slightly lower absorption co-efficient than pure CuO (phase percentage, CuO 100%).

From the figure 4.6. we can see that at 525 nm wavelength only Germanium has an absorption co-efficient higher than S3. But it is a matter of fact that Germanium has never been used as an absorption layer of a solar cell due to its less efficiency according to Shockley- Queisser Limit. The cheap alternate for the absorption layer is silicon, which is industrially accepted, has much lower absorption coefficient than S3.

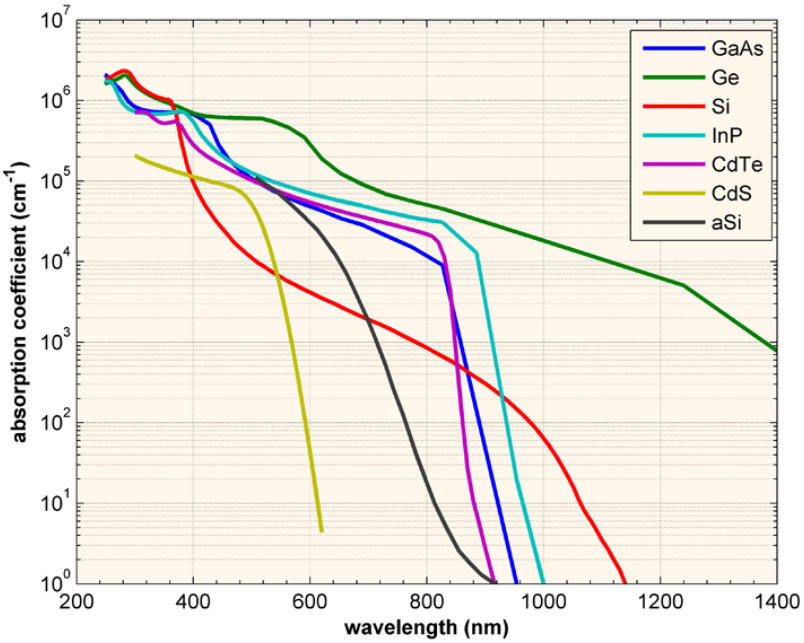

Figure 4.6. Comparison of the absorption coefficient of different materials [9]

Band Gap. The band gap (E_g) of a semiconductor is very important in electronic and optical properties. It is the energy gap between a valence band and a conduction band. To excite an electron for conducting, a minimum change in energy is needed and this minimum change in energy is called the Band Gap. It determines how much energy is needed from the sun for the

electron in the junction to move and conduct current, and so it is quite an important parameter for the material to be considered as a potential absorption layer.

Tauc Relation: $\alpha h\nu = A (h\nu - E_g)^n$ [30]

For direct bandgap, n =1/2

For indirect bandgap, n =2

To determine the energy gap, most authors use the model for direct interband transitions:

$\alpha h\nu = A (h\nu - E_g)^{1/2}$

in which *hν* is photon energy, n is index of refraction, and α is the absorption coefficient. In this approximation, $(\alpha h\nu)^2$ should be a linear function of *hν.* This model may not be suited to wide band gap materials because the optical absorption band edge is strongly disturbed by a coulombic electron- hole interaction leading to the excitonic effect.

The calculated band gaps for the samples are listed in table 4.3. The procedure showed in Figure 4.7 is used for the calculation of band gap from Tauc plotting. From the table it can be said that the sample 3 has a direct band gap of 1.80 eV and an indirect band gap of 1.11 eV. As the degree of linearity is higher in the direct band gap calculation than the indirect band gap calculation, it indicates the possibility of prevalence of the direct band gap in sample 3. The estimated indirect optical bandgap energy of CuO is about 1.11 eV while the calculated energy of the optical band gap CuO in the case of direct transitions is in the range (1.45–1.60) eV and the direct optical bandgap for undoped Cu_2O is 2.1eV [31]. It is important for optoelectronics device to have direct bandgap. But CuO being an indirect bandgap material and Cu_2O being a direct bandgap material offers a wider range of bandgap with possibility of both direct and indirect band gap for the samples with phase mixture.

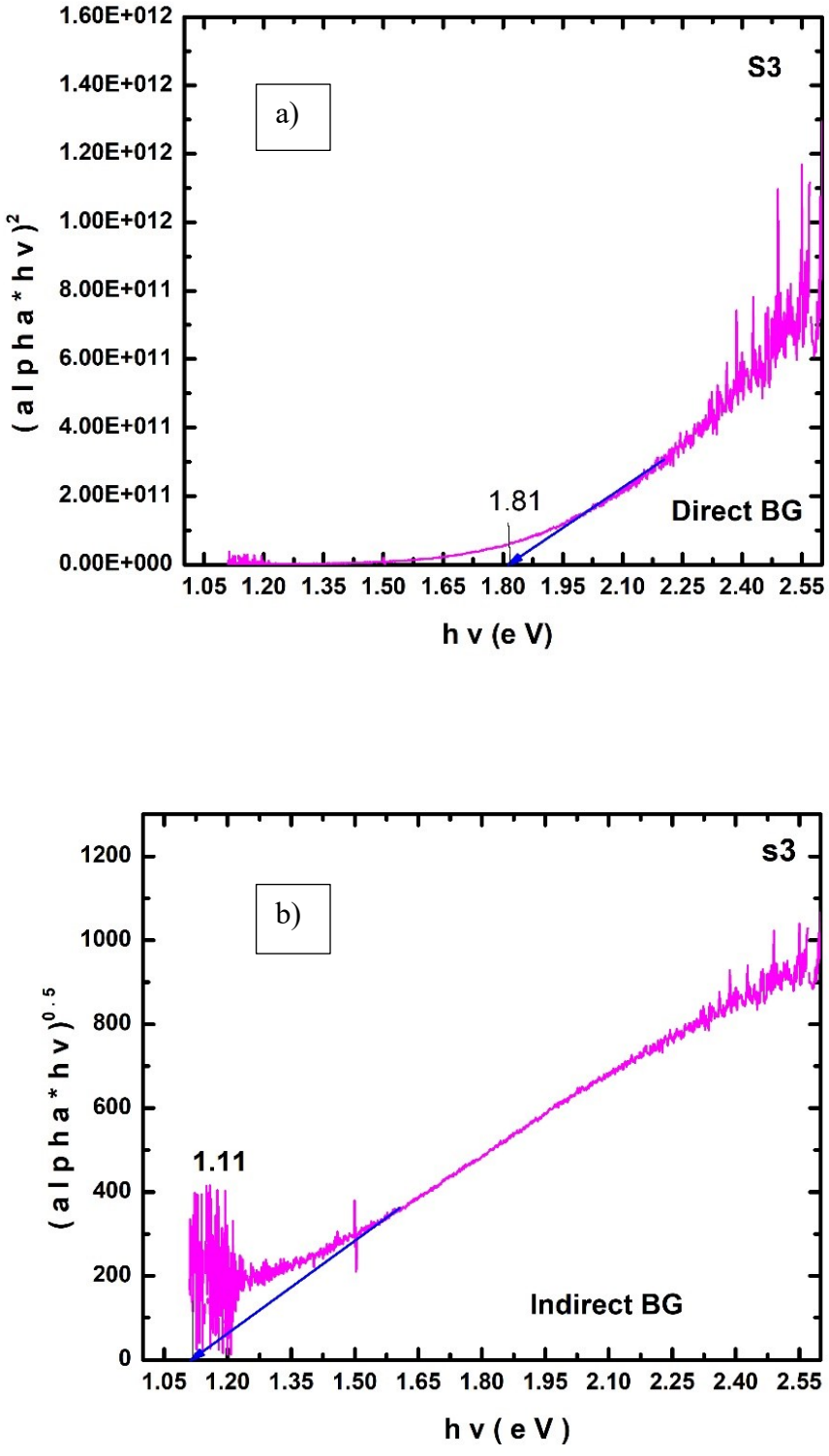

Figure 4.7. Tauc plot for sample S3 providing (a) direct and (b) indirect band gaps

Table 4.3. Direct and Indirect Band Gap calculated for the samples

Sample no.	Direct BG (eV)	Indirect BG (eV)
S1	2.29	1.41
S2	1.95	1.22
S3	1.81	1.11
S4		1.1

According to structural and optical properties of CuO thin films CuO thin films have a high absorbance in the visible spectrum (85–90%), which decreases with increasing wavelength. The phase mixture of CuO and Cu_2O can offer increment in this absorbance due to the tuning in band gap. Sample 4 which has the highest absorption co-efficient, has indirect band gap 1.11 which is very close to CuO. It is known that the change in E_g of the film material may be due to the presence defects, small grain size, semiconductor degeneracy which are introduced by the presence of two different phases. If the phase mixture has higher BG than the pure CuO/Cu_2O, that indicates Band gap widening which we can see in the samples. And so high transmittance was affected by band gap widening which occurred due to phase mixture [32]

Electrical Characterization

AC Resistance Measurement. Resistance of all these 4 samples were measured from I-V curve. To measure the I-V curve, a two-probe resistance measurement workstation was used. A circuit diagram for the AC measurement is given in Figure 4.8. A function generator was used as the AC voltage source, and a storage oscilloscope was used to view the output. LABVIEW program was used to fetch the graph to a computer.

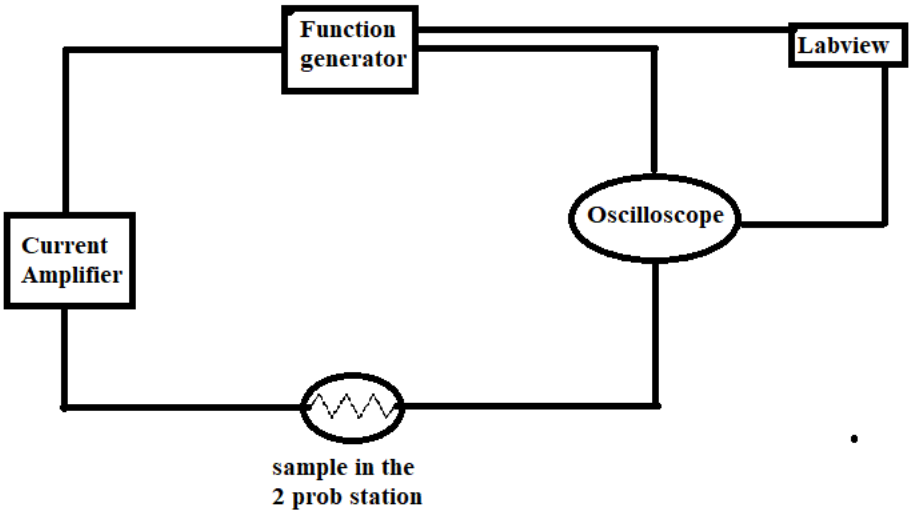

Figure 4.8. Circuit for AC measurement

A voltage in the range of 0 to 5 V was supplied from the function generator to each sample (in case of S1, the supplied voltage was very low, 0.2 V as the sample resistance was much lower than other samples), and the supplied voltage and respective current were recorded in the storage oscilloscope. The graphs from the oscilloscope were imported to a computer using a LABVIEW program which are shown in Figure 4.9. and Figure 4.10.

Due to the AC response of all these 4 samples, the visible change in current is very small. So, no conclusion can be drawn from these ac response graphs.

R Measurement DC. A two probe R measurement station is used along with Parameter Analyzer 4200 to measure the resistance of all 4 samples and the values are listed in table 4.4.

One crucial parameter for being considered as a potential material for absorption layer is good to moderate conductivity. That is why it is crucial to measure resistivity of any material to know it's conductivity before considering that material for solar cell application.

This experiment is done in the presence of light and without light from the "Newport 69907 light Analyzer" was used to measure the resistance of each sample with and without light.

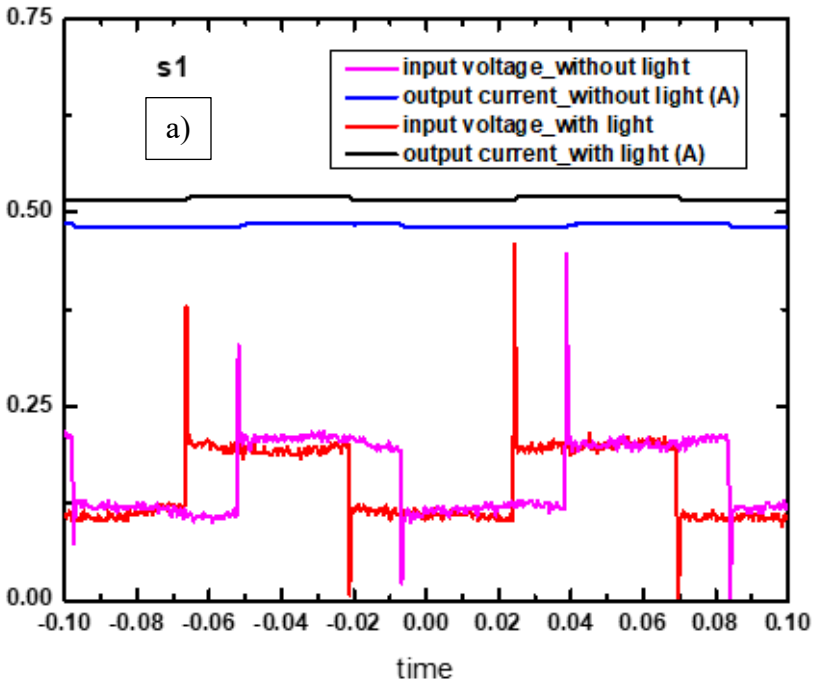

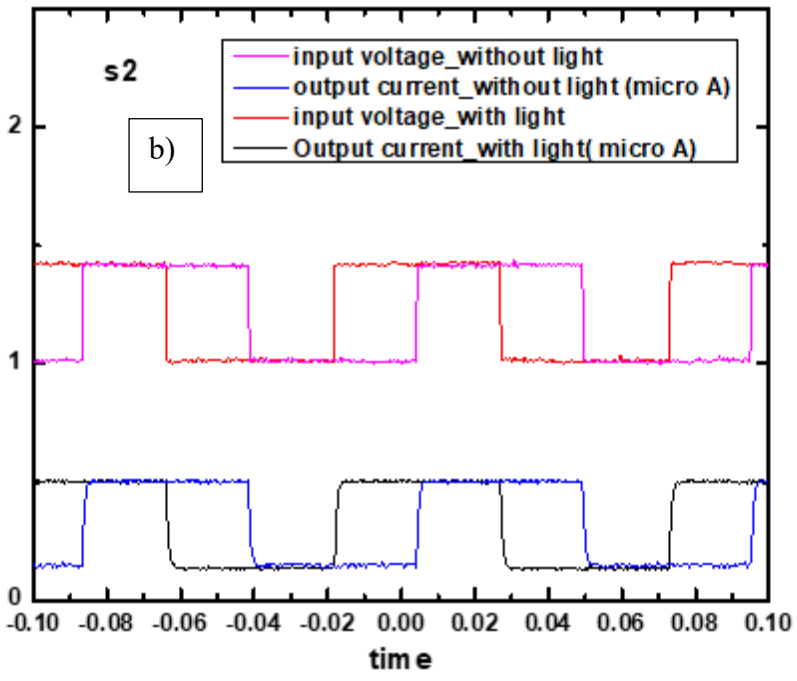

Figure 4.9. Plotting of the AC measurement with and without light for a) S1 and b) S2

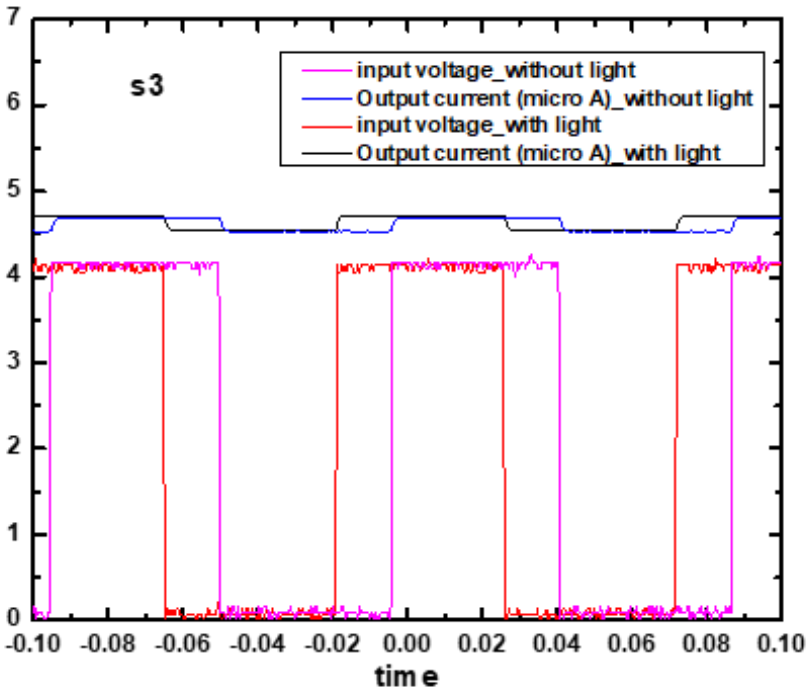

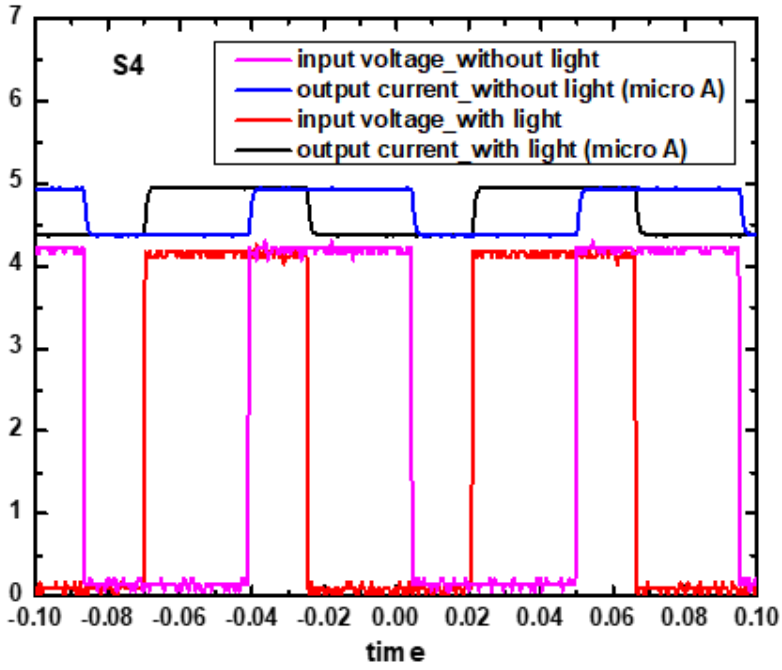

Figure 4.10. Plotting of the AC measurement with and without light for a) S3 and b) S4

Table 4.4. Resistivity measurement of all samples (with and without light)

Sample no.	Resistance Without light(Ω) For DC measurement	Resistance with light (Ω) For DC measurement	Decrease (in %)	Resistivitywith light (Ω/cm)	Resistivity without light (Ω /cm)
S1	187	186	0.53	3.75E-5	3.75E-5
S2	1.1123E+6	1.1005E+6	1.06	0.22	0.223
S3	2.5605E+7	2.4282E+7	5.17	4.8564	5.121
S4	7.1278E+6	6.9752E+6	2.14	1.395	1.425

The parameter analyzer applies a dc voltage in the range of from -2V to +2 V (in the case of S1, from -0.5 V to +0.5 V due to its low resistance) across each sample and a corresponding current flow through each sample which gives the linear I-V curve which indicates the resistive nature of each sample. The slope of the curve gives the value of the resistance of each sample which are shown in figure 4.11. and 4.12. From all the samples, S3 has shown the most distinguished change in the resistance due to light.

S1 has incredibly low resistance which can be attributed to the 49% of metallic copper traced from the XRD data. So, even if with exceptionally low resistance, this high amount of metallic copper is a huge drawback for solar cell applications. Also, high reflectance and poor transmittance (< 15 %), due to the presence of metallic Cu overall makes this S1 impractical as an option for the material of absorption layer of solar cell [33]. On the other hand, S3 has a moderate resistance without light and the decrease in the resistance with light is 5.2% which is very expectant

for application as absorption layer. Moreover, the high absorption coefficient value makes it an overall potential material for solar cell application.

Photosensitivity. is a term used to describe sensitivity to ultraviolet rays (UV) from sunlight and other sources of light, such as fluorescent light indoor. It is defined as the ratio of the change in the conductivity to the dark value ($\Delta\sigma_{light}/\sigma_{dark}$) [34] It is a matter of fact that when semiconductive layers are used to serve as an absorbing material for solar cells as thin film, a small photosensitivity is quintessential. Photoconductivity is an optical and electrical phenomenon in which a material becomes more electrically conductive owing to the absorption of electromagnetic radiation, such as visible light, ultraviolet light, infrared light, or gamma radiation. When light is absorbed by a material, the number of free electrons and holes increases and raises its electrical conductivity. To cause excitation the light that strikes the semiconductor must have enough energy to raise electrons across the band gap or to excite the impurities within the band gap. Photocurrent is the electric current that flows as a result of a photoconductivity or a photovoltaic effect [35]

As we can see from the calculation, in table 4.5, S3 has the highest value of photosensitivity other than S1. As discussed before, S1 has an abundant amount of copper which makes it ineligible for use as an element of the absorption layer of a solar cell. So, from all the sample, S has the best photosensitivity to be implemented as an absorption layer.

High photosensitivity of the films can be attributed to the grain size enhancement by the phase. Due to the phase variance in the samples, the band gap and absorbance varied as well. And as the phase mixture of S3 enhanced the optical property and conductivity, the photosensitivity of S4 increased as well . The photosensitivity is in the range of 0.01-0.06 [36] which typical for potential material suitable for the use as an absorption layer in solar cell.

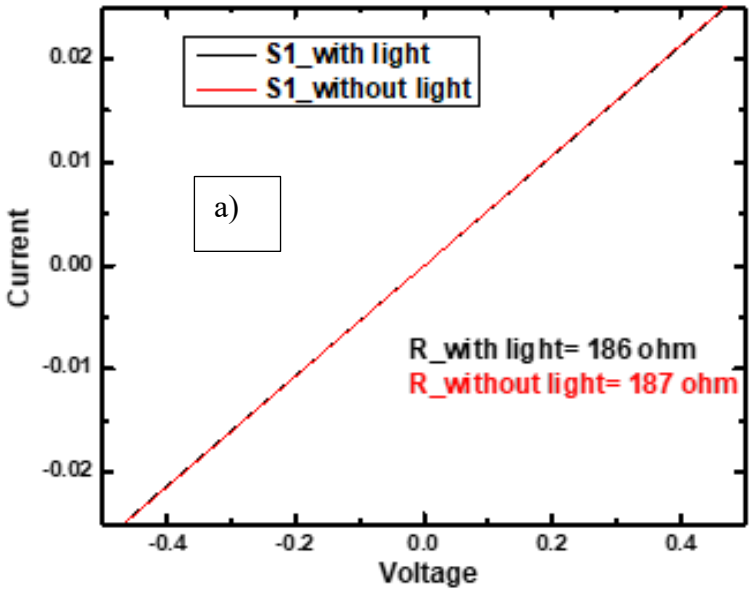

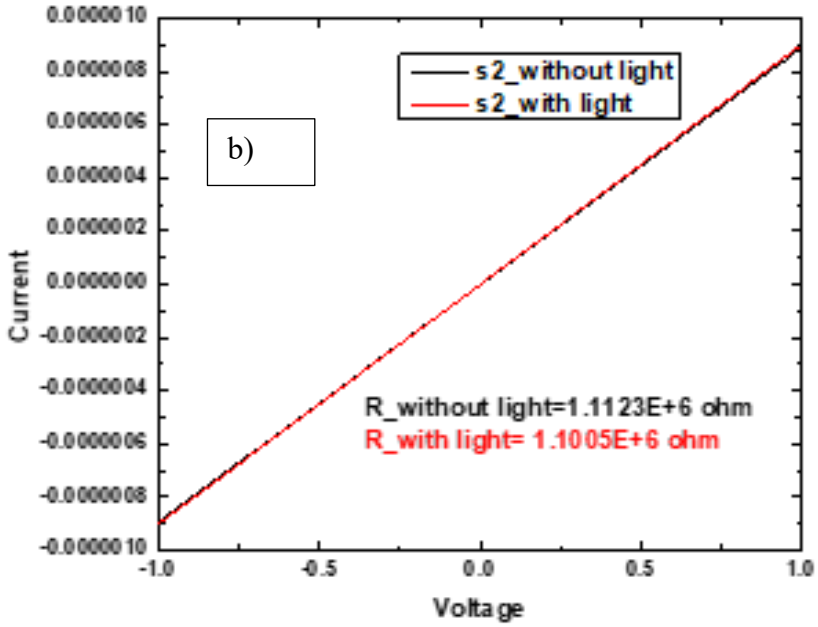

Figure 4.11. Plotting of the DC measurement with and without light for a) S1 and b) S2

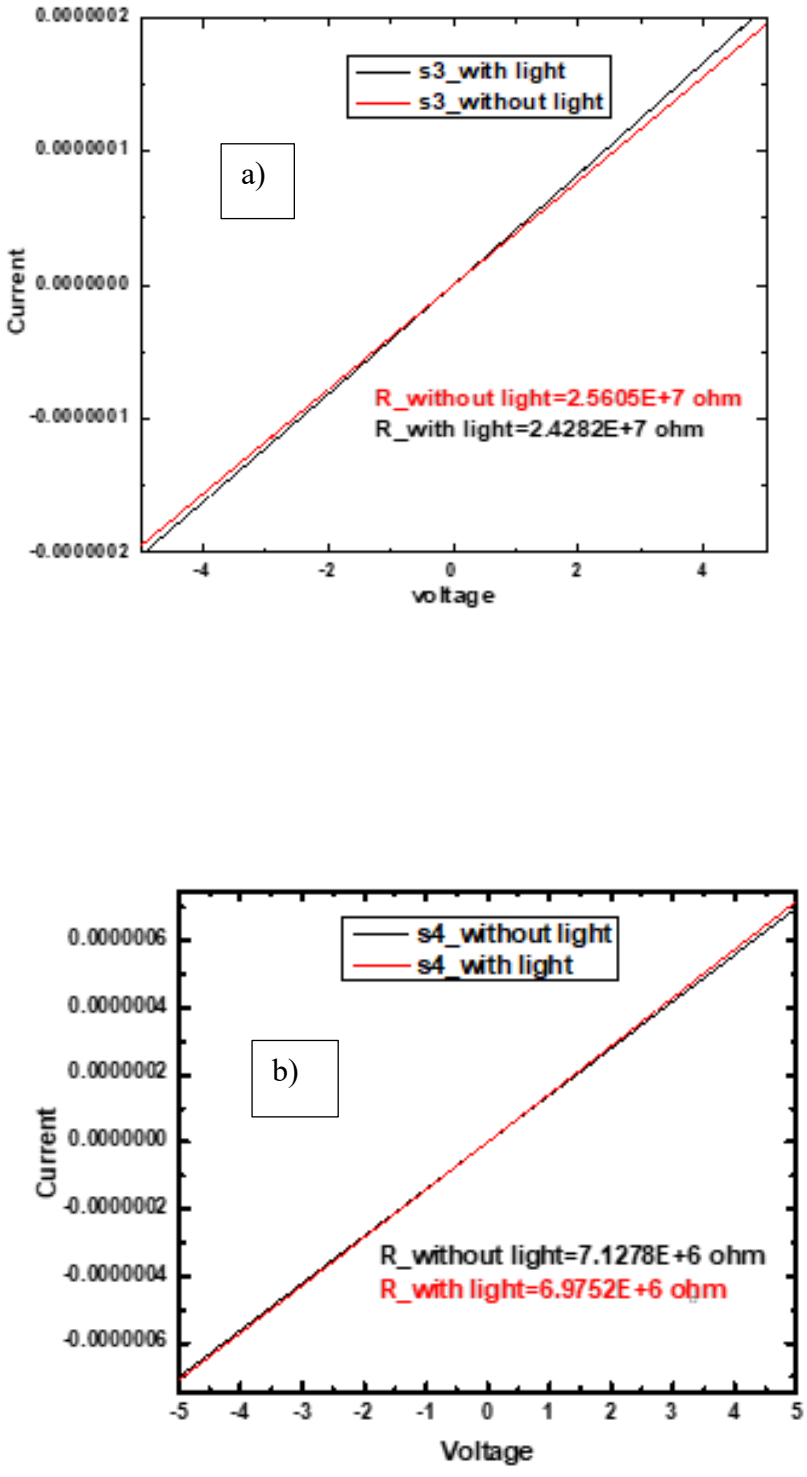

Figure 4.12. Plotting of the DC measurement with and without light for a) S3 and b) S4

Table 4.5. Photosensitivity of the samples

Sample no.	Conductivity From DC measurement with light (S/m)	Conductivity from DC measurement without light (S/m)	Photo-sensitivity
S1	2.6E+5	5.35E+6	0.95140
S2	4.5	4.495	1.1E-3
S3	0.2059	0.195	0.05294
S4	0.7168	0.7015	0.021810

Light Response with Time. With the intention of having a more detailed idea of the behavior of the resistance of S3 with the presence of light, the current response with light of S3 is observed with time at a constant voltage and the output is shown in Figure 4.13. The Parameter Analyzer 4200 was used to supply a constant voltage of 1 V, and the "Newport 69907 light source" was used to provide light. A cycle of light off for every 50 second with on for 2 second afterward was conducted for total 225 seconds and the result is shown in the graph. From the graph, we can see that there is an increase in current every 50 s with the decrease in resistance due to the presence of light. This indicates that S3 is very responsive to light which makes it a good candidate for the absorption layer of a solar cell.

Raman Spectroscopy

The Raman spectra of the three samples (S1, S2, S3) are shown in Figure 4.15.a), 4.15.b) and 4.16 respectively. The Voigt peak fitting was used to analyze Raman data in Labspec 5

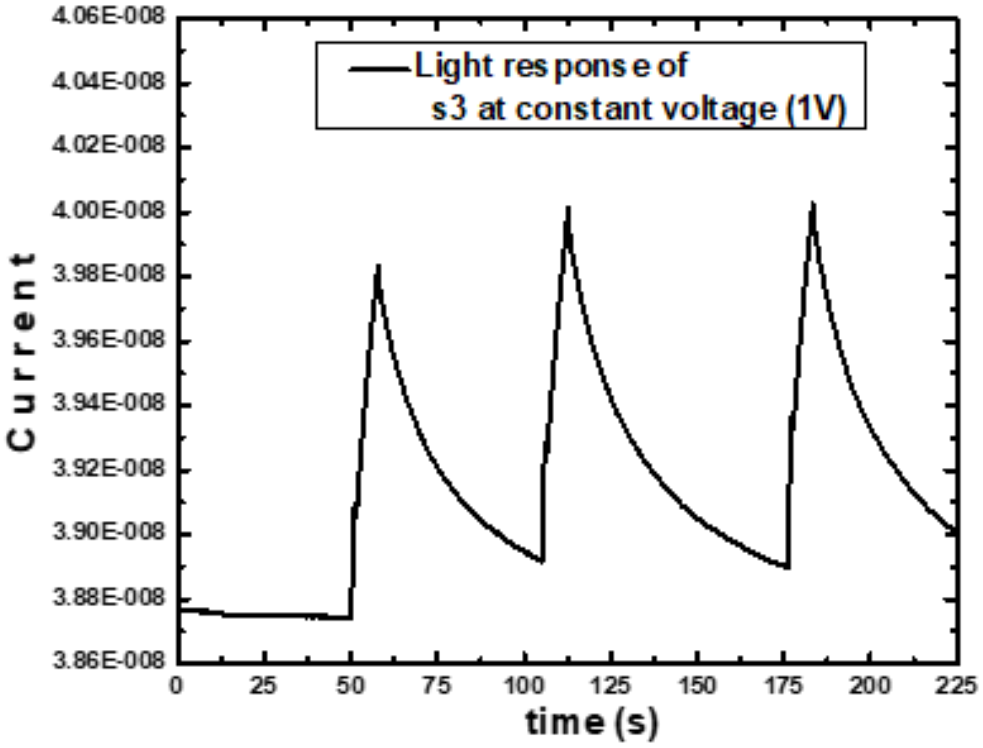

Figure 4.13. Light response of sample 3 with time at a constant voltage (1 V)

software. CuO belongs to the C6 2h space group with two molecules per primitive cell and has 12 phonon branches because there are four atoms in the primitive cell. Optical phonon modes have total nine zone-centers which have symmetries denoted by $4A_u + 5B_u + A_g + 2B_g$. From these symmetries only three modes are Raman active which are ($1A_g + 2B_g$). These three modes can be found at 296 cm^{-1} (A_g), 346 cm^{-1} (B_{1g}), and 631 cm^{-1} (B_{2g}) in the Raman spectra as shown in figure 4.14. [37]

Cu_2O has a cubic structure, and the space group is Pn3m. Its primitive cell contains two Cu_2O units. Total 15 optical phonon modes and three acoustic phonon modes are present for Cu_2O. But the only Raman active mode is T_{2g} symmetry due to the vibrations belonging to the

Table 3. Calculated Frequencies ω_c of Zone-Center (Γ) Phonons for Tenorite CuO, As Compared to Experimental Values (ω_e) in cm^{-1}[a]

sym	activity	ω_c	ω_e (this work)	ω_e (other)
B_u	IR	141		147[21,24]
A_u	IR	164		161[21,24]
A_g	Raman	319	296	301–303[27,44]
A_u	IR	327		321[21,24]
B_g	Raman	382	346	348–350[27,44]
A_u	IR	457		478[21,24]
B_u	IR	503		533[21,24]
B_u	IR	568		587[21,24]
B_g	Raman	639	631	633–636[27,44]

[a]Symmetries (sym) and Raman or infrared activity are indicated.

Figure 4.14. Positions of the Raman peaks for CuO [37]

threefold degenerate. There are two silent modes namely A_{2u} and E_u. The mode intensities and the number of observed modes may vary in this work [4].

As shown in the figure 4.17., Raman spectra of glass has strong and wide peak in the range of 550-700 and 900-1200. From the graph of the Raman spectra of S2 and S3 we can see that glass has strong background that makes it difficult to clearly detect the presence of CuO and Cu_2O in those ranges. It can be implied that glass has high intensity broadened Raman peak in the range of 600- 1100 cm^{-1} which makes it difficult to distinguish the peak of CuO and Cu_2O from the peak of glass due to strong background. From figure 4.11.a) the presence of a high intensity peak around 200 can be seen. The presence of this peak causes fainting the peaks from glass. The probable reason for this particular high intensity peak is the presence of a plasmon peak from

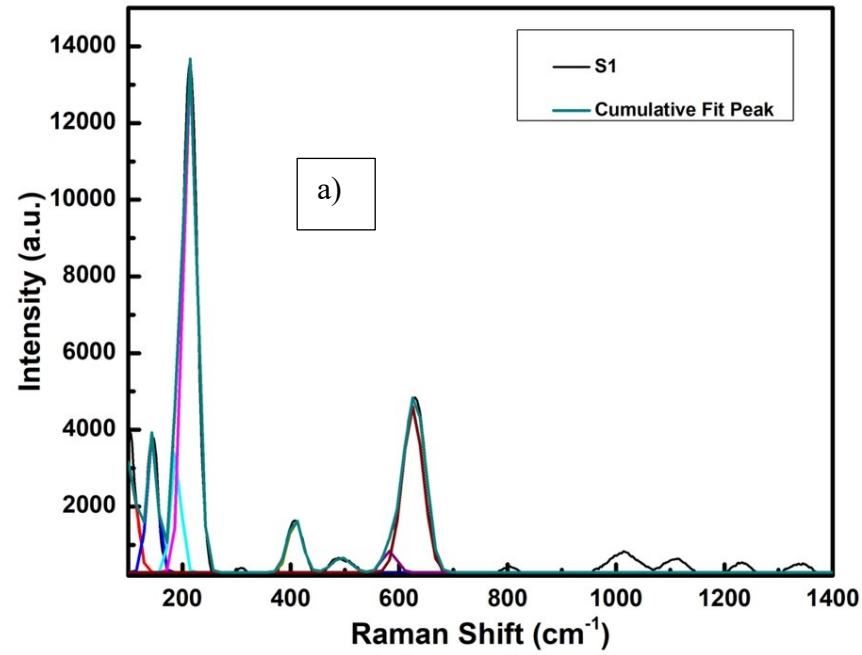

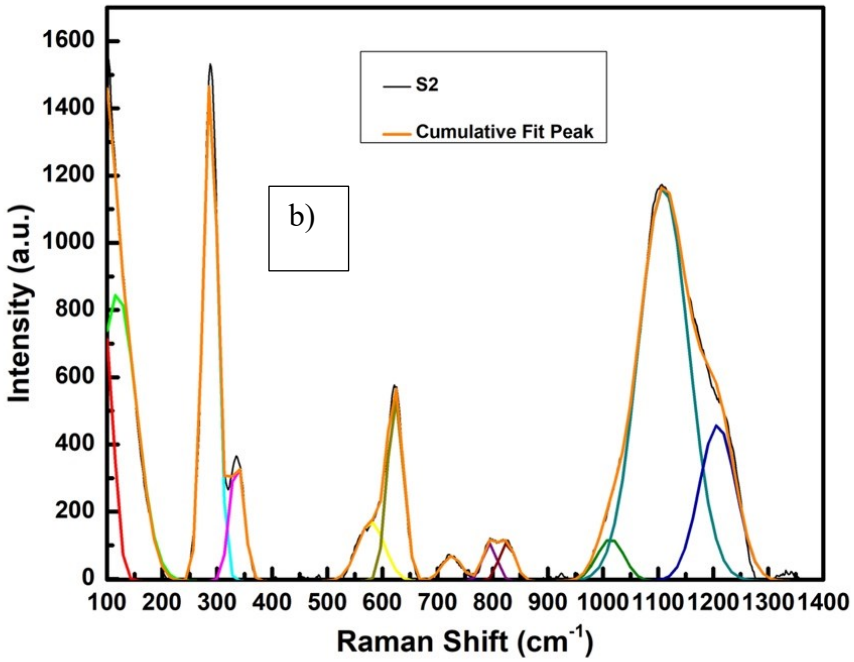

Figure 4.15. Raman spectra of a) S1 and b) S2

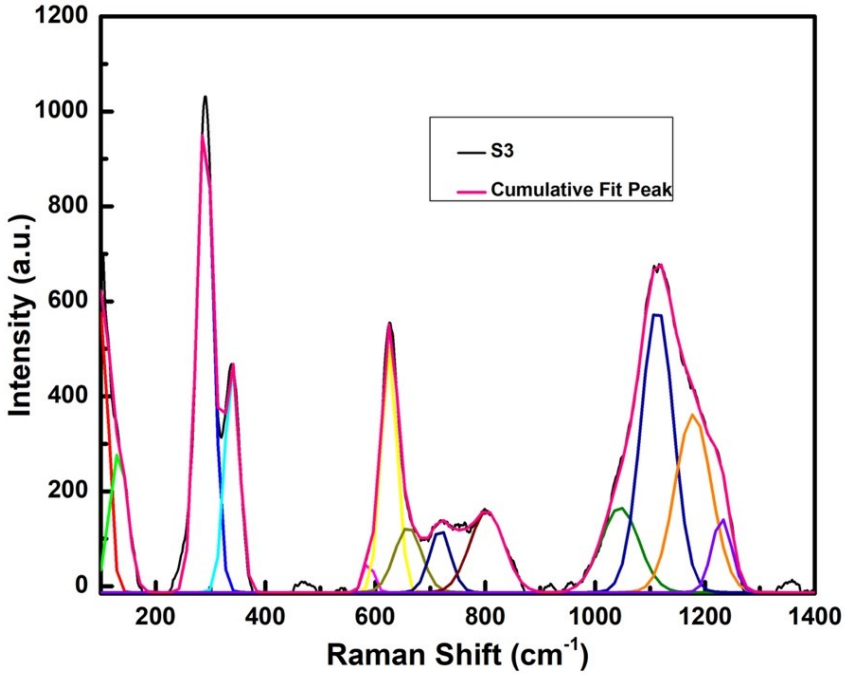

Figure 4.16. Raman spectra of sample 3

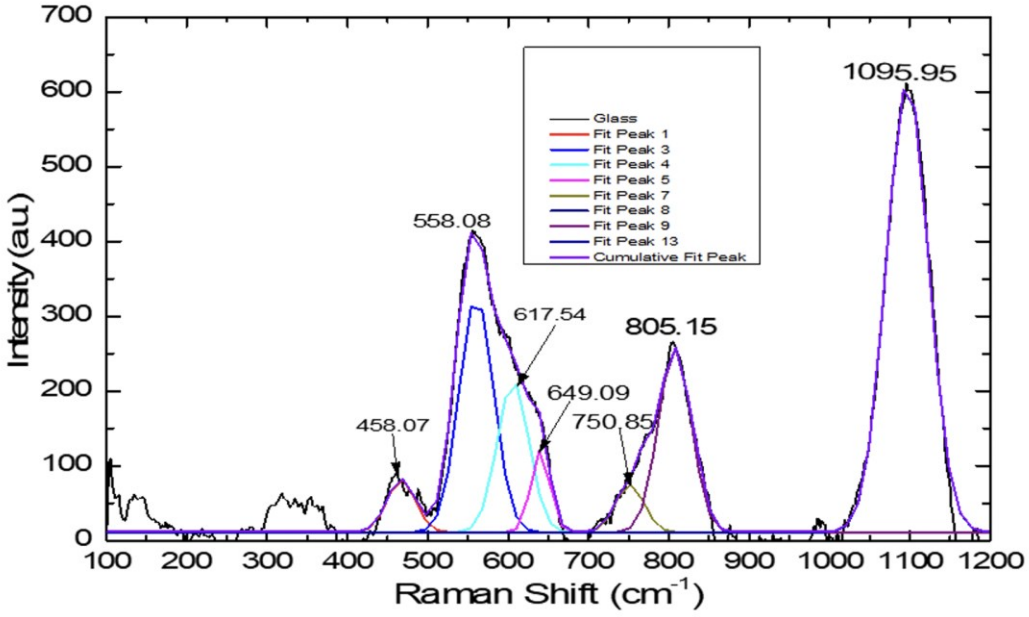

Figure 4.17. Raman spectra of glass

copper which is abundant particularly in sample 1.

From the reference of the Raman spectra of Cu_2O it can be said that it has Raman peaks at 109, 154, 218,308, 436 and 515 before 600 cm^{-1}. Figure 4.11. b) shows that S2 has convoluted peak around 150 and 300 cm^{-1} which can be an indication to the presence of Cu_2O as well. However, due to the strong background from the glass, it is tough to accurately predict which vibrational mode of CuO and Cu_2O are present in the samples. In the Raman spectra of S3 in figure 4.11.c) peak around 600- 700 cm^{-1} can be from either B_{2g} mode of CuO (around 631 cm^{-1}) or T_{2g} mode of Cu2O (around 650 cm^{-1}). Overall, the Raman data is an indication of the presence of CuO and Cu_2O but for the phase percentage, deduction was solely dependent on the XRD data.

Scanning Electron Microscopy

SEM images of the three selective phase mixture copper oxide thin film samples S1, S2, and S3 are shown in Figure 4.18. All the samples have a regular thin film like structures with traces of random grains which are very small. S3 has large circular grain compared to other samples.

Summary

Thin films of phase mixtures of copper oxides with high absorption coefficient and optical response on electrical conductivity have been synthesized using PLD. The solar absorption coefficient of the thin films with phase mixture of copper oxide is significantly large (3.25E+5 cm^{-1}) as compared to standard pure CuO (1.0E+5 cm^{-1}) which can be attributed to the change in energy band gap and a particular phase mixture of copper oxides (CuO 87.30%,

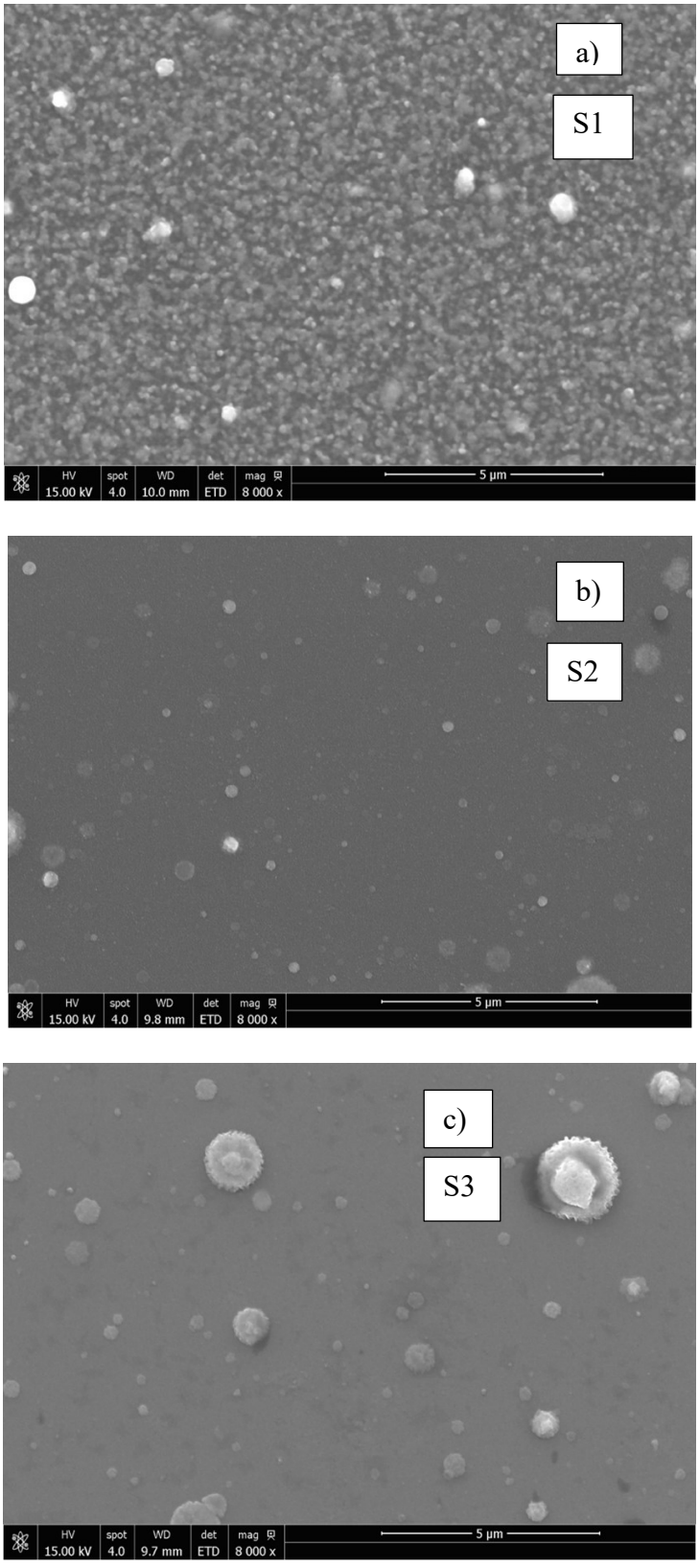

Figure 4.18. SEM images of a) sample 1, b) sample 2 and c) sample 3

Cu_2O 12.70%). The ability to create and recreate phase mixture of copper oxides with large optical absorption coefficient combined with moderate photo-response on electrical conductivity can lead to develop solar cell using phase mixture of oxide semiconductors.

COMPUTATIONAL STUDY ON THE PHASE MIXTURE USING DFT

Introduction

CuO has a monoclinic structure, and Cu_2O has a cubic structure with space groups c12/c1 and Pn3m, respectively. Both compounds can be used as a semiconductor and vastly used as an active layer of a solar cell. There are many studies previously on them as an individual absorption layer. The phase mixture (weight percentage) can increase efficiency by providing wider range of band gap. CuO being indirect band gap material and Cu_2O being direct band gap material, the possibility of having wider range cannot be ignored. The unit cell of CuO and Cu_2O were collected from **Materials Project website** and then the supercell of CuO was created using **OVITO visualization software** and all of them are shown in Figure 5.1. Previous studies have shown band gap with low value (0.95 eV) [38]. using the Hubbard potential value 4.5 eV.

Methodology

Density functional theory (DFT) calculations were performed using Quantum Espresso with a plane-wave basis set (pw) and ultrasoft pseudo-potentials under periodic boundary condition. In case of the exchange-correlation (XC) functional, for both DFT and DFT+U, The Perdew-Burke-Ernzerhof (PBE) was used. The kinetic energy cutoff is chosen as 40 Ry due to the limitation with capability of the computer.

The calculation begins with the electronic structure of unit cell of CuO and Cu2O to predict theoretical band gap using DFT+U method. The Hubbard potential value was set to 7 eV. For the calculation of DOS, projected DOS, and band structure, ‘Tetrahedra’ was used as the occupancy type. The DOS, PDOS, and band structure was plotted using Origin Pro**.**

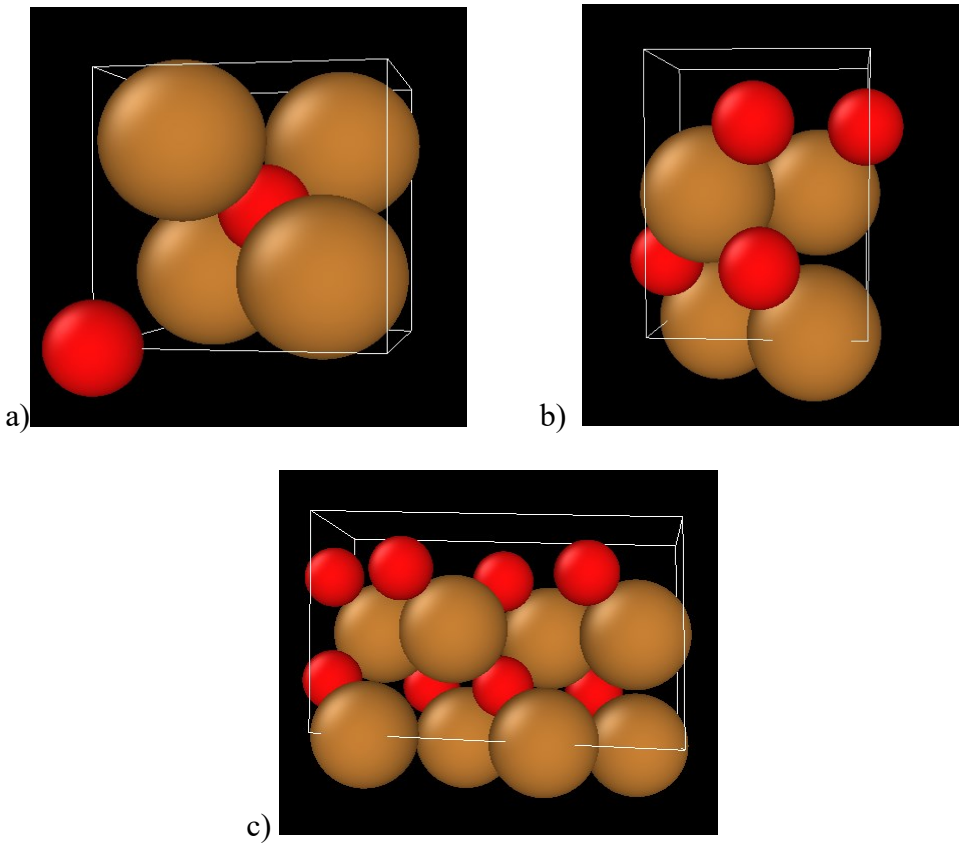

Figure 5.1. Unit cell of a) Cu_2O and b) CuO, and c) super cell of CuO

Study of Unit Cell of Cu_2O and CuO

The interaction between Cu^{+} and O^{2-} based on a simple closed-shell model is inadequate. However, it still can offer an insinuation about the interaction, and so what might happen during the phase transition. In order to understand how the band structure might change due to change in phase, at first it is necessary to know how the band structure looks like in a pure material. That is why at first the unit cells of Cu_2O and CuO were studied, and their DOS and PEDOS were observed along with the band structures to have an overall idea.

Study of the Unit Cell of Cu_2O. Using Quantum Espresso, the DOS, PEDOS and band structure of Cu2O were observed where The Monkhorst-Pack k-point sampling was set as

10×10× 10, and the energy cutoff was chosen as 40 Ry. LDA+U correction was used, and Hubbard Potential value was set as 7 eV. The observed data are shown in figure 5.2. and 5.3.

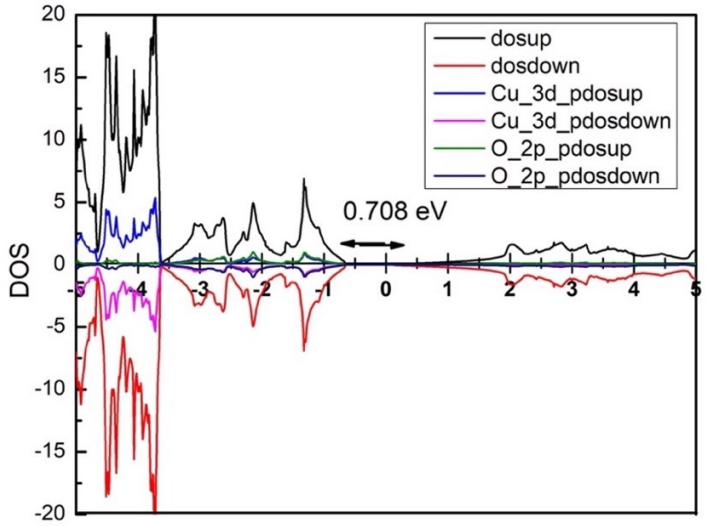

Figure 5.2. Cu (3d) and O (2p) PEDOS and Cu2O DOS from DFT with LDA+U, U = 7 eV

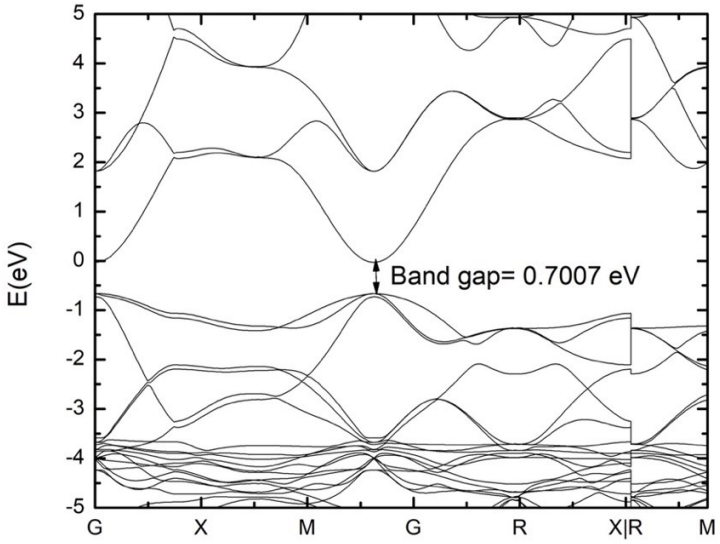

Figure 5.3. Band structure of Cu_2O from DFT with LDA+U, U=7 eV

The plotting of band structure for Cu_2O indicates a direct band gap of 0.708 eV. This is higher than the band gap calculated for Cu_2O in [39]. They got a direct band gap with value 0.65 eV using a Hubbard potential, U=4.5 for LDA+U correction. The plotting of DOS along with the PEDOS of Cu (3d) and O (2p) indicates the same band gap which is direct in nature.

Study of unit cell of CuO. CuO has indirect band gap which makes the calculation for band structure of CuO more complicated. One study [40] got an indirect band gap of value 1.48 eV for CuO using U = 7 eV and cut off E as 400 eV. they varied the Hubbard potential from no potential to 9 eV and got the no band gap for no Hubbard potential whereas the highest band gap for U = 9 eV. But using cut off E as 400 eV and Hubbard potential, U = 7 eV for LDA+U yielded the result shown in figure 5.4 and 5.5. [40]showed in their study that using cut off E as 500 eV and U = 8 eV is yielding a band of 1.98 eV which is even slightly higher than the recognized band gap of CuO (1.1-1.4 eV). From this data it could be assumed that increasing the cut off energy and the Hubbard potential might easily solve the problem. But [41] showed in their study that this trade of is not simple linear. The function, as well as the cut off energy and the potential value all are playing a role here, and yet the band gap can be low.

In “Materials Project” as shown in Figure 5.6. the band structure for CuO has a similar fermi level sinked inside the valence band instead of being in between valence band and conduction band which is shown in figure 5.6. So, it can be said that this kind of ambiguity is another aspect of the band structure of CuO which might be caused by the indirect nature of the band gap [42]

Study of Super Cell of CuO

For this specific study, study of the change in the band gap due to phase transition is transition from CuO to Cu_2O, a supercell of CuO was studied and oxygen vacancy was introduced. The

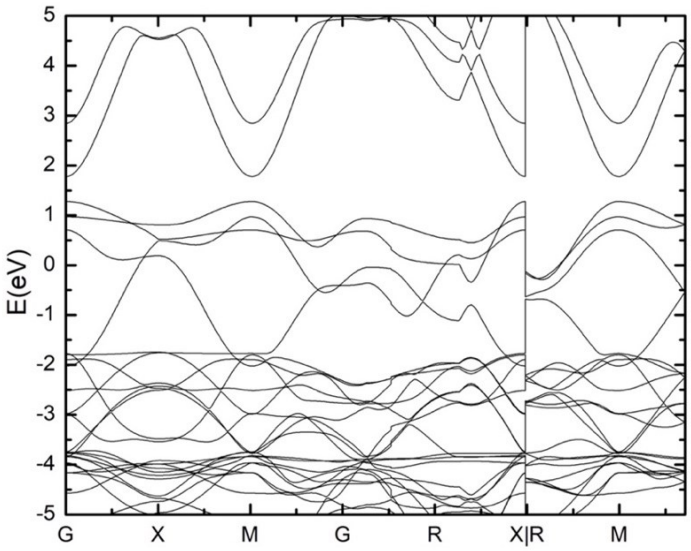

Figure 5.4. Band structure of unit cell of CuO from DFT with LDA+U, U=7 eV

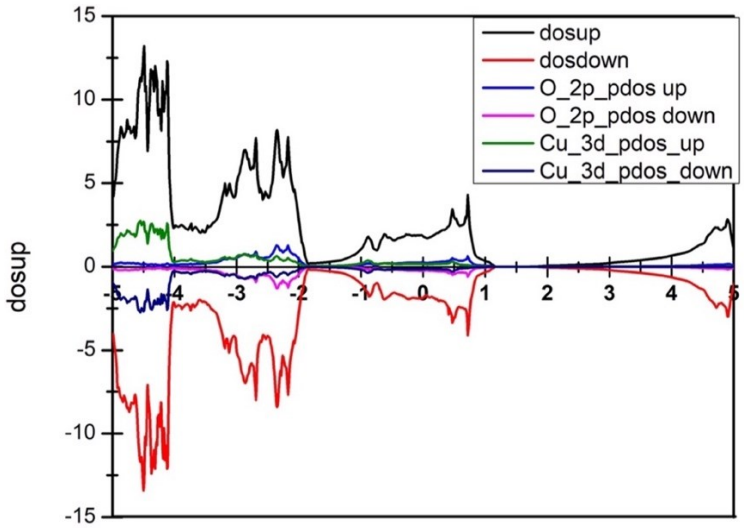

Figure 5.5. Cu (3d) and O (2p) PEDOS and CuO (unit cell) DOS from DFT with LDA+U, U = 7 eV

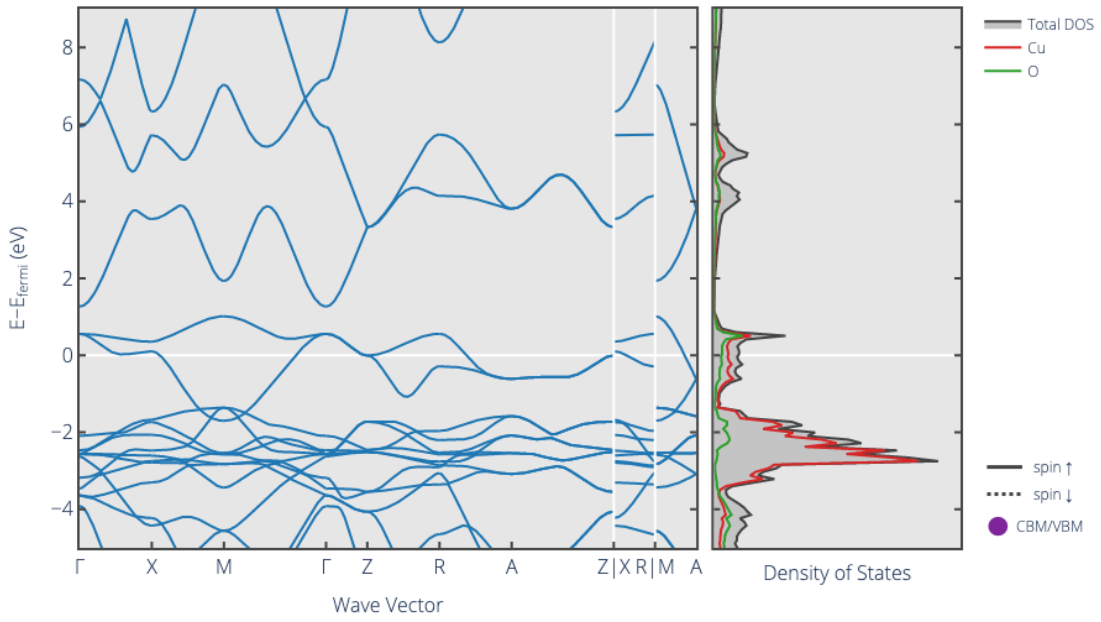

Figure 5.6. Similar band structure from reference

Monkhorst–Pack k-point sampling scheme was applied, with 10 irreducible k- points for (2 × 1 × 1) cell expansion. An oxygen vacancy was introduced in the supercell using OVITO. Then the Band structure, DOS and PEDOS was studied for both the supercell with and without vacancy to see the effect of the oxygen vacancy on the band formulation.

Study of the Supercell of CuO with No Vacancy. The supercell of CuO yielded similar band structure where the fermi energy level is located inside the valence band which is shown in figure 5. 7. Figure 5.8 is the plotting of the PEDOS of copper 3d band and oxygen 2p band along with the DOS which verifies that the fermi level is inside the valence band.

Study of the Supercell of CuO with Vacancy. When an oxygen vacancy was introduced in the mentioned position in figure 5.9, the followed band structure and DOS and PEDOS of Cu 3d and O 2p band were observed as shown in Figure 5.10. and 5.11. respectively. As found before from the no vacancy demonstration, there were not any visible band gap found. However, close range

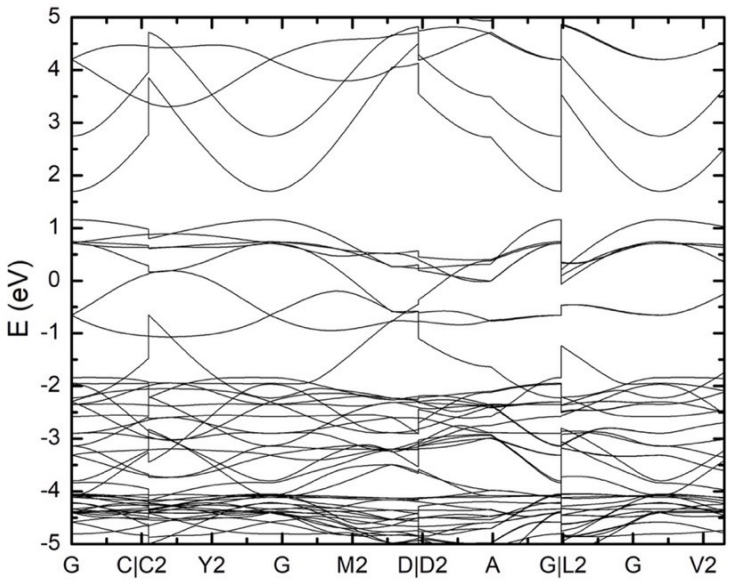

Figure 5.7. Band structure of unit cell of CuO (no vacancy) from DFT with LDA+U, U=7 eV

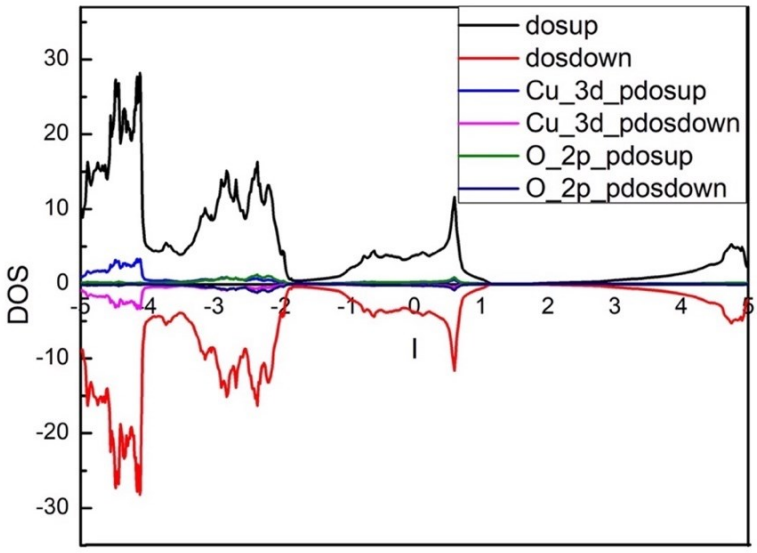

Figure 5.8. Cu (3d) and O (2p) PEDOS and CuO (supercell no vacancy) DOS from DFT with LDA+U, U=7 eV

observation indicated some interesting phenomena.

Discussion. when compared the PEDOS of the supercell of CuO before and after introducing the oxygen vacancy in closer range as demonstrated in figure 5.12., it was observed that the intensity of the PEDOS of Oxygen 2p band is decreasing in some particular area and affecting the shape of the PEDOS of Copper 3d band. The overall DOS is becoming wider which is an indication of the introduction of new band. In figure 5.12.a. it is observed that the DOS is becoming wider in the range of 1-3 eV which was absent before introducing the oxygen vacancy. Moreover, the close-range comparison between the band structure in figure 5.13. indicates that some new bands are being introduced in the valence band while some other bands are changing the trajectory. The overall conduction is being shifted upper ward and a new band is being introduced at the fermi level in the valence band region.

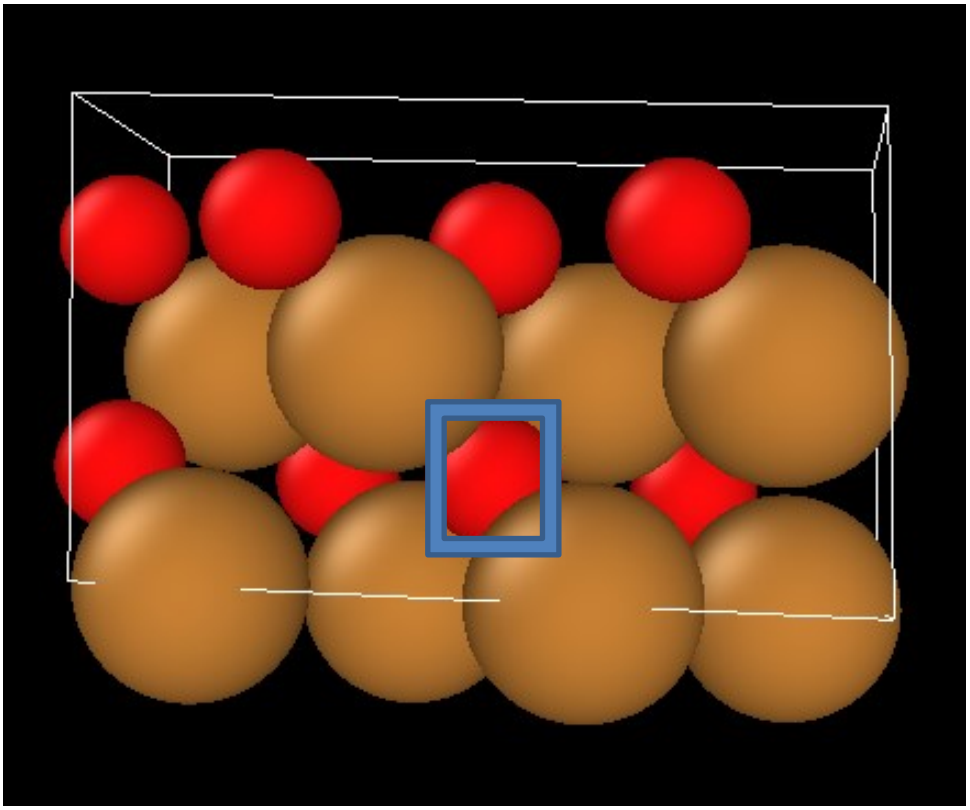

Figure 5.9. Position of the oxygen vacancy in supercell of CuO

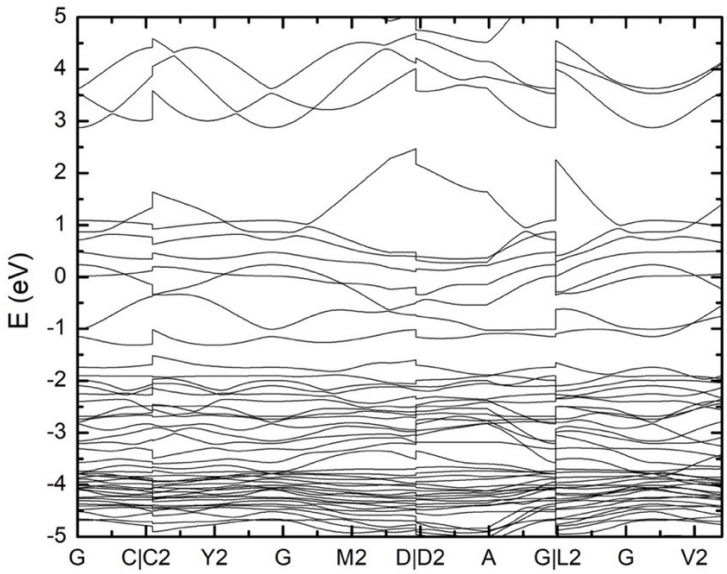

Figure 5.10. Band structure of super cell of CuO (with oxygen vacancy) from DFT with LDA+U, U = 7 eV

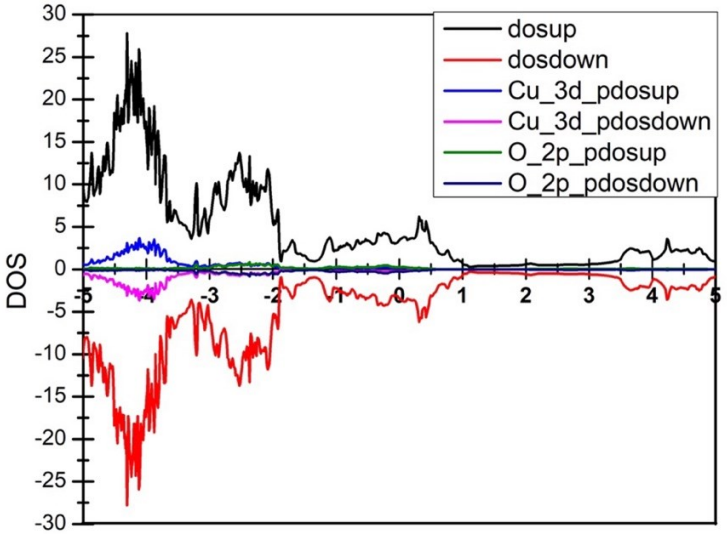

Figure 5.11. Cu (3d) and O (2p) PEDOS and CuO (supercell with oxygen vacancy) DOS from DFT with LDA+U, U=7 eV

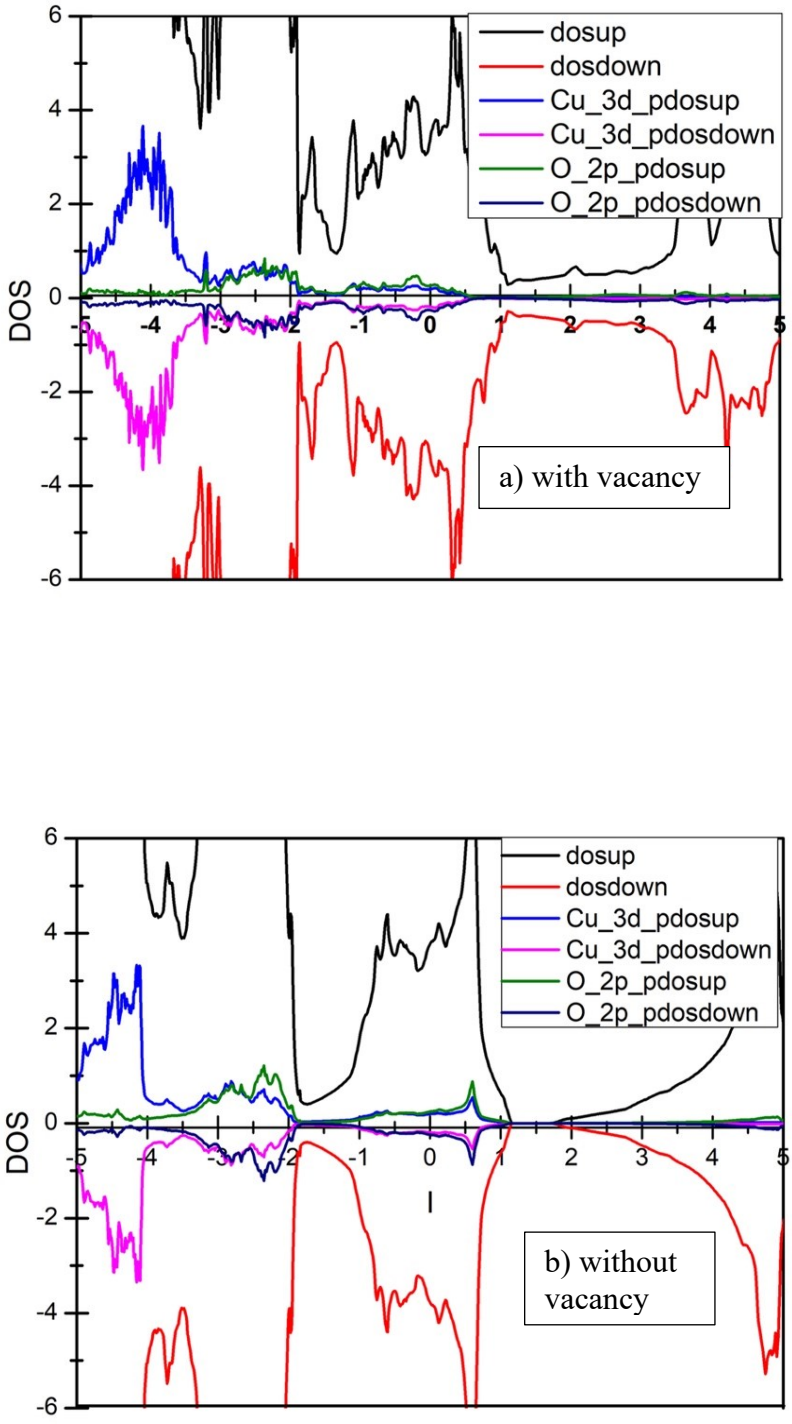

Figure 5.12. Comparison between PEDOS of supercell of CuO a) with vacancy and b) without vacancy

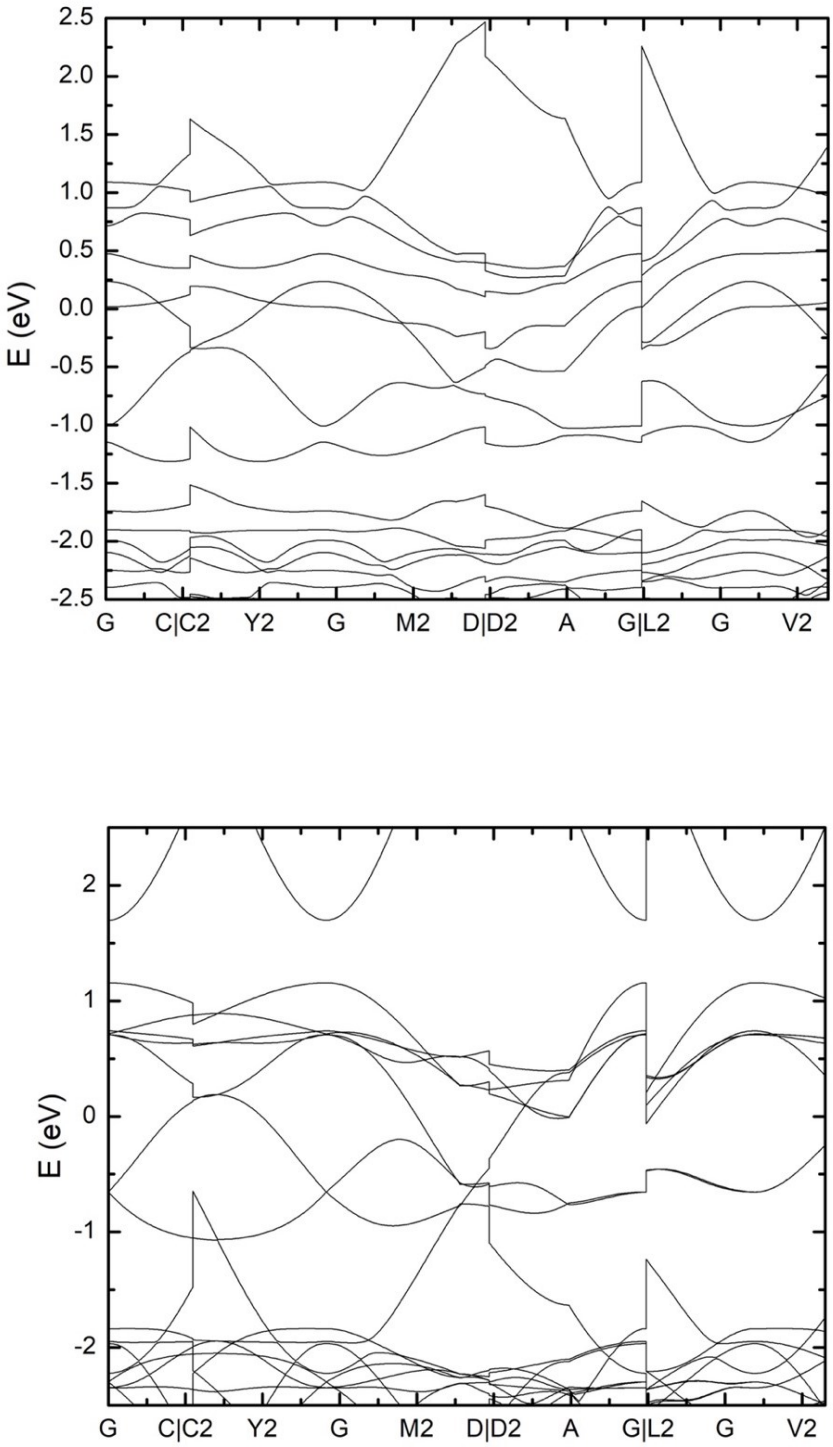

Figure 5.13. Comparison between the band structure of supercell of CuO a) without vacancy and b) with oxygen vacancy

Summary

This study on the band structure of Cu_2O and CuO unit cell indicates that Cu_2O has more predictable band structure due to having direct band gap while the band structure of CuO demonstrates ambiguity due to having an indirect band gap. So, having the exact band gap of CuO from computational study requires more resources. The introduction of oxygen vacancy in CuO manifest how the domination of the PEDOS of oxygen 2p band is decreasing which introduces more bands in the valence band region and shifting the conduction band region. Due to limited resources this study used ($2 \times 1 \times 1$) mesh of CuO as a supercell. Higher mesh with better correction method might provide a better understanding on the effect of oxygen vacancy and thus about the phase transition.

CONCLUSION AND FUTURE WORK

Conclusion

Firstly, the goal of figuring out the optimum parameter for varying the percentage of the phase mixture of copper oxide in bulk was studied. Keeping the pressure constant, the temperature and time was varied one at a time to see the effect on the percentage of the phase mixture of copper oxide. The experimental work showed that the temperature range of 350° - 400°C is optimum for the phase transition reactions of copper oxide in presence of H_2/Ar gas. Higher temperature capitulate in metallic form, Cu, and lower temperature might not provide any reaction at all. Time was varied in range of 15 minutes to 1 hour (60 minutes), but more precise tuning can provide better insight into the control for tuning. However, the non-uniform film of bulk copper oxide was non- suitable for optical and electrical characterization.

In order to achieve both the mixture of phase and eligibility for characterization, pulsed laser deposition technique was adapted, and deposition was done on glass substrates using copper target in presence of O_2 gas at 400°C. Different percentages of phase mixture of copper oxide thin films were successfully obtained from depositions at varied O_2 pressure. The percentage phase mixture was obtained from TOPAS analysis of the XRD data of each sample. Then optical and electrical characterization were done using UV-VIS, two probe R measurement, and current measurement with time. Additional Raman characterization and SEM were conducted. The optical and electrical characterization manifested that the sample with a particular percentage of the phase mixture of copper oxide (CuO 87.30%, Cu_2O 12.70%) gives a balanced combination of both the absorption co-efficient and photo-response in electrical conductivity. This particular phase mixture demonstrated high absorption coefficient (3.25E+5

cm^{-1}) which is higher than accepted absorption co-efficient of CuO (1.0E+5 cm^{-1}) for solar cell application. Finally, it's very responsive current flow with time depending on the presence of light at a constant voltage makes it a potential material for the active layer of a solar cell.

With an aim to have deeper understanding of the mechanism of phase transition, the band structure of pure CuO and Cu_2O (unit cell) were attempted for study, and an approach of introducing oxygen vacancy in super cell of CuO was taken. However, though Cu_2O ascribed a band gap of 0.707 eV, due to the limitation of resources, and complex band structure of CuO due to indirect nature of the band gap, no acute band gap was retrieved from the study. The fermi level was found shifted inside the valence band instead of being in a gap between the valence and conduction band. However, as the matter of concern of this study was having the apprehension of the change in band structure due to phase transition, the change in band structure after introducing oxygen vacancy was studied anyway, and it was found that the intensity of the PEDOS of oxygen 2p band decreased. Some new bands were introduced in the valence band while the conduction band had an upper shift. This result helps understand the change in band structure due to phase transition which is playing a vital role in improving the absorption co-efficient and providing a balance between the good absorption property and moderate conductivity.

Future Work

There are still some limitations to address to implement this material for solar cell application. For example, repeatability of the percentage of the phase mixture, tuning the percentage of phase mixture after synthesizing the copper oxide phase mixture thin film using

pulsed laser deposition are some matters of concern in order to adapt this material as an option for an active layer.

One possible solution to this issue is to use reduction annealing on the thin film to vary the percentage of the phase mixture. The idea is to create the thin film of copper oxide using Cu target and air annealing the film to have 100% CuO in the film. After that, reduction annealing at 350°C- 400°C for different time duration might yield different percentage of the phase mixture of copper oxide in the film.

With farther study on the tuning and repeatability, it is possible to consider this phase mixture of copper oxide as a prospective material for absorption layer of a solar cell and implement in an actual solar cell. The proposed structure in Figure 6.1. can be used for constructing an actual solar cell where the phase mixture of copper oxide can be used as an active layer.

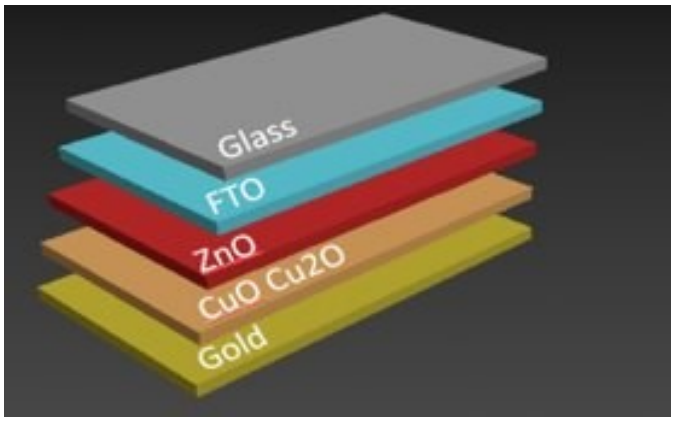

Figure 6.1. Proposed structure of a solar cell with the phase mixture of copper oxide as an active layer

REFERENCES

[1] R. M. H. H. Jayarathne, D. P. Pitigala, V. * P. S. Perera, Electronic and structural properties of Cu2O polycrystalline thin films grown on adhesive copper tape, Proceedings Tech. Sessions 35 (2019) 31–38.

[2] Crystal-structure-of-Cu2O-a-Crystal-structure-of-Cu2O-b-2D-projection-view-of-64.

[3] B. K. Meyer, Binary copper oxide semiconductors: From materials towards devices, Phys. Status S. (B) Basic Res. 249 (2012) 1487–1509, doi:10.1002/pssb.201248128.

[4] O. It, A. D. Melting, E. Haikkola, Cu2O Char. Ref. (2008).

[5] B. Balamurugan, B. R. Mehta, Optical and structural properties of nanocrystalline copper oxide thin films prepared by activated reactive evaporation, Thin Solid Films 396 (2001) 90–96, doi: 10.1016/S0040-6090(01)01216-0.

[6] H. J. Li, Growth behavior and optical properties of N-doped Cu2O films, Thin Solid Films 520 (2011) 212–216, doi: 10.1016/j.tsf.2011.07.037.

[7] J. L. Gray, Phys. Solar Cell (2011), doi: 10.1002/9780470974704.ch3.

[8] C. Wadia, A. P. Alivisatos, D. M. Kammen, Materials availability expands the opportunity for large-scale photovoltaics deployment, Environmental Sci. Tech. 43 (2009) 2072–2077, doi: 10.1021/es8019534.

[9] N. M. Ahmed, Z. Sauli, U. Hashim, Y. Al-douri, Investigation of the absorption coefficient, refractive index, energy band gap, and film thickness for Al0.11Ga0.89N by optical transmission method, Int. J. Nanoelec. Mater. 2 (2009) 189–195.

[10] L. C. Olsen, R. C. Bohara, M. W. Urie, Explanation for low-efficiency Cu2O Schottky-barrier solar cells, Appl. Phys. Lett. 34 (1979) 47–49, doi: 10.1063/1.90593.

[11] C. A. Wolden, Photovoltaic manufacturing: Present status, future prospects, and research needs, J. of Vac. Sci. Tech. A: Vac. Surf. Films 29 (2011) 030801, doi: 10.1116/1.3569757.

[12] Y. Ievskaya, R. L. Z. Hoye, A. Sadhanala, K. P. Musselman, and J. L. MacManus-Driscoll, Fabrication of ZnO/Cu2O heterojunctions in atmospheric conditions: Improved interface quality and solar cell performance, Solar E. Mater. Solar Cells 135 (2015) 43–48, doi: 10.1016/j.solmat.2014.09.018.

[13] T. K. S. Wong, S. Zhuk, S. Masudy-Panah, G. K. Dalapati, Current status and future prospects of copper oxide heterojunction solar cells, Mater. 9 (2016) 1–21, doi: 10.3390/ma9040271.

[14] K. Akimoto, S. Ishizuka, M. Yanagita, Y. Nawa, G. K. Paul, T. Sakurai, Thin film deposition of Cu2O and application for solar cells, Solar E. 80 (2006) 715–722, doi: 10.1016/j.solener.2005.10.012.

[15] A. E. Rakhshani, Preparation, characteristics and photovoltaic properties of cuprous oxide-a review, S. State Elec. 29 (1986) 7–17, doi: 10.1016/0038-1101(86)90191-7.

[16] B. Yan, J. Yang, S. Guha, Amorphous and nanocrystalline silicon thin film photovoltaic technology on flexible substrates, J. Vac. Sci. Tech. A: Vac. Surf. Films 30 (2012) 04D108, doi: 10.1116/1.4707154.

[17] D. A. R. Barkhouse, O. Gunawan, T. Gokmen, T. K. Todorov, D. B. Mitzi, Yield predictions for photovoltaic power plants:empirical validation,recent advances and remaining uncertainties, Progress in Photovoltaics: Res. Appl. 20 (2015) 6–11, doi: 10.1002/pip.

[18] S. Masudy-Panah, G. K. Dalapati, K. Radhakrishnan, A. Kumar, H. R. Tan, Reduction of Cu-rich interfacial layer and improvement of bulk CuO property through two-step sputtering for p -CuO/ n -Si heterojunction solar cell, J. Appl. Phys. 116 (2014) 7, doi: 10.1063/1.4893321.

[19] L. L. Hench, J. O. N. K. West, The Sol-Gel Process, (1990) 33–72.

[20] I. Boyd, D. B. Chrisey, Pulsed laser deposition of thin films (2004), doi:10.1887/0750306076/b1388v3c9.

[21] O. D. Neikov, N. A. Yefimov, Nanopowders, Handbook of Non-Ferrous Metal Powders (2019) 271–311, doi: 10.1016/B978-0-08-100543-9.00009-9.

[22] R. K. Singh, J. Narayan, Pulsed-laser evaporation technique for deposition of thin films: Physics and theoretical model, Phys. Rev. B 41 (1990) 8843–8859, doi:10.1103/PhysRevB.41.8843.

[23] K. Instruments, User's Manual *P4200A-900-01B* Model 4200A-SCS Parameter Analyzer (2017), [Online]. Available: www.tek.com/keithley

[24] P. J. Worsfold, UV—visible Spectroscopy and its Applications, Analy. Chimica Acta 284 (1993) 245, doi: 10.1016/0003-2670(93)80039-n.

[25] M. Birkholz, A Practical Guide to X-Ray Crystallography of Biomacro- molecules Surface and Thin Film Analysis Electron Accelerators as X-Ray Sources Microscopic X-Ray Fluorescence Analysis X-Ray Spectrometry X-ray Characterization of Materials (2006).

[26] A. Bogner, P. H. Jouneau, G. Thollet, D. Basset, C. Gauthier, A history of scanning electron microscopy developments: Towards 'wet-STEM' imaging, Micron. 38 (2007) 390–401, doi: 10.1016/j.micron.2006.06.008.

[27] A. Bhaumik, A. M. Shearin, R. Patel, K. Ghosh, Significant enhancement of optical absorption through nano-structuring of copper based oxide semiconductors: Possible future materials for solar energy applications, Phys. Chem. 16 (2014) 11054–11066, doi: 10.1039/c4cp00827h.

[28] C. Guillén, J. Herrero, Single-phase Cu2O and CuO thin films obtained by low-temperature oxidation processes, J. Alloys Comp. 737 (2018) 718-724.

[29] C. Malerba, F. Biccari, C. Leonor Azanza Ricardo, M. D'Incau, P. Scardi, A. Mittiga, Absorption coefficient of bulk and thin film Cu2O, Solar E. Mater. Solar Cells 95 (2011) 2848–2854, doi: 10.1016/j.solmat.2011.05.047.

[30] N. Ghobadi, Band gap determination using absorption spectrum fitting procedure, Int. Nano Lett. 3 (2013) 2–5, doi: 10.1186/2228-5326-3-2.

[31] S. Masudy-Panah, K. Radhakrishnan, A. Kumar, T. I. Wong, R. Yi, G. K. Dalapati, Optical bandgap widening and phase transformation of nitrogen doped cupric oxide, J. Appl. Phys. 118 (2015) 22, doi: 10.1063/1.4936318.

[32] H. J. Li, Growth behavior and optical properties of N-doped Cu2O films, Thin Solid Films 520 (2011) 212–216, doi: 10.1016/j.tsf.2011.07.037.

[33] S. A. Studenikin, N. Golego, M. Cocivera, Optical and electrical properties of undoped ZnO films grown by spray pyrolysis of zinc nitrate solution, J. Appl. Phys. 83 (1998) 2104–2111, doi: 10.1063/1.366944.

[34] A. Morales-Acevedo, Effective absorption coefficient for graded band-gap semiconductors and the expected photocurrent density in solar cells, Solar E. Mater. Solar Cells 93 (2009) 41–44, doi: 10.1016/j.solmat.2008.02.015.

[35] R. Mondal, Molecular design for improved photovoltaic efficiency: Band gap and absorption coefficient engineering, J. Mater. Chemistry 19 (2009) 7195–7197, doi: 10.1039/b915222a.

[36] K. Bindu, P. K. Nair, Semiconducting tin selenide thin films prepared by heating Se-Sn layers, Semicond. Sci. Tech. 19 (2004) 1348–1353, doi: 10.1088/0268-1242/19/12/003.

[37] A. Bhaumik, A. M. Shearin, R. Patel, K. Ghosh, Significant enhancement of optical absorption through nano-structuring of copper based oxide semiconductors: Possible future materials for solar energy applications, Phys. Chem. 16 (2014) 11054–11066, doi: 10.1039/c4cp00827h.

[38] A. Živković, A. Roldan, N. H. de Leeuw, Density functional theory study explaining the underperformance of copper oxides as photovoltaic absorbers, Phys. Rev. B 99 (2019) 1–10, doi: 10.1103/PhysRevB.99.035154.

[39] F. Pei, Electronic and optical properties of noble metal oxides M2O (M = Cu, Ag and au): First-principles study, J. Korean Phys. 55 (2009) 1243–1249, doi: 10.3938/jkps.55.1243.

[40] M. Nolan, S. D. Elliott, The p-type conduction mechanism in Cu2O: A first principles study, Phys. Chem. 8 (2006) 5350–5358, doi: 10.1039/b611969g.

[41] K. Harun, N. A. Salleh, B. Deghfel, M. K. Yaakob, A. A. Mohamad, DFT + U calculations for electronic, structural, and optical properties of ZnO wurtzite structure: A review, Res. Phys. 16 (2019) 102829, doi: 10.1016/j.rinp.2019.102829.

[42] Y. Hinuma, G. Pizzi, Y. Kumagai, F. Oba, I. Tanaka, Band structure diagram paths based on crystallography, Comp. Mater. Sci. 128 (2017) 140–184, doi: 10.1016/j.commatsci.2016.10.015.